SAND-75-0668
Unlimited Release

TRANSMISSION AND COMPRESSION OF AN INTENSE RELATIVISTIC ELECTRON BEAM PRODUCED BY A CONVERGING ANNULAR DIODE WITH RETURN CURRENT FEEDBACK THROUGH THE CATHODE:

PART II - THE EXPERIMENTS

J. G. Kelly, R. L. Schuch

Prepared by Sandia Laboratories, Albuquerque, New Mexico 87115 and Livermore, California 94550 for the United States Atomic Energy Commission under Contract AT (29-1)-789

Printed February 1976

Sandia Laboratories

SF 2900 Q(7-73)

When printing a copy of any digitized SAND Report, you are required to update the markings to current standards.

Issued by Sandia Laboratories, operated for the United States Energy Research and Development Administration by Sandia Corporation.

NOTICE

This report was prepared as an account of work sponsored by the United States Government. Neither the United States nor the United States Energy Research and Development Administration, nor any of their employees, nor any of their contractors, subcontractors, or their employees, makes any warranty, express or implied, or assumes any legal liability or responsibility for the accuracy, completeness or usefulness of any information, apparatus, product or process disclosed, or represents that its use would not infringe privately owned rights.

Printed in the United States of America
Available from
National Technical Information Service
U. S. Department of Commerce
5285 Port Royal Road
Springfield, VA 22151
Price: Printed Copy $6.50; Microfiche $2.25

SAND-75-0668
Unlimited Release
Printed February 1976

TRANSMISSION AND COMPRESSION OF AN INTENSE RELATIVISTIC ELECTRON BEAM PRODUCED BY A CONVERGING ANNULAR DIODE WITH RETURN CURRENT FEEDBACK THROUGH THE CATHODE: PART II - THE EXPERIMENTS

J. G. Kelly
Radiation Physics Division 5423
and
R. L. Schuch
Beam Source Applications Division 5232

Sandia Laboratories
Albuquerque, NM 87115

ABSTRACT

The complete results of the experiments with the converging annular diode with return current feedback through the cathode (Triax) are reported herein. The diode was designed to focus a relativistic high-current electron beam to a small focus. It did confirm the Triaxial theory detailed in Part I,[1] and it did achieve a factor of 10 areal compression with 50 percent efficiency (which was below expectations). There were two principal reasons for this shortfall. First, the rapid diode plasma motion of 10 cm/μsec that was discovered necessitated the use of larger A-K gaps than expected and led to thicker beam sheets than are needed for good focusing. Second, the intrinsic angular spread of the electrons, even from the best cathode surfaces, introduced excessive angular momentum into the beam so that only a minor portion of the electrons could reach the axis.

However, the yield of useful information about diode physics in general and about the influence of prepulse, the role of diode plasmas, the motion of energetic beams within conducting boundaries, diode emission properties, and diode diagnostic techniques in particular has had a significant and useful impact on the electron beam program at Sandia.

CONTENTS

		Page
I	INTRODUCTION	7
II	THE DESIGN AND FABRICATION OF THE REBA TRIAX	9
	Features of the REBA Accelerator	9
	The Design of the First REBA Diode	9
	Cathode Emitters	14
III	TESTS WITH THE ORIGINAL TRIAX DESIGN	17
	Tests Without the Feedback System	17
	First Tests of the Triax System	21
	Summary and Conclusions about the First Triax Diode	33
IV	THE MODIFIED REBA TRIAX DIODE	35
	Modifications of the REBA Triax	35
	Electron Pinhole and Mapping Diagnostics	38
	The Investigations of the Triax Diode Output	40
	The Search for a Narrower Beam and the Problems with Prepulse	48
	Transport and Compression in Cones	58
	The Effect of Radial Vanes in the Channel	65
	Discussion and Conclusions about the REBA Triax System	68
V	THE HYDRA TRIAXIAL DIODE	73
	The Hydra Accelerator and the Design of the Diode	73
	The Experiments with the Hydra Diode	79
	Conclusions about the Hydra Experiments	86
VI	DISCUSSION AND GENERAL CONCLUSIONS ABOUT THE TRIAX SYSTEM	88
REFERENCES		91

FIGURES

Figure		Page
2.1	REBA Diode with Prepulse Switches	10
2.2	Sketch of the Triax and the Transport Cones	11
2.3	Machine Drawing of the Triax Diode	13
2.4	Cross Section of Ring Cathode Emitters	16
3.1	Photograph of Inner Cone Spall Marks	18
3.2	Beam Profile without Feedback, 90 μ	19
3.3	Photograph of Pinhole Plates after a Shot	19
3.4	Pinhole Exposure of Electron Angular Distribution from the Shot without Feedback	20
3.5	Beam Profile with Maximum Feedback, 90 μ	22
3.6	Photograph of the Radial Razor Cathode Ring	24
3.7	Beam Profile with Feedback, Correct Injection, 3 Torr	25
3.8	Turning of Electrons in the Cathode Ring B Field	26
3.9	Photograph of the Cathode Shank with Copper Filled Corners	27
3.10	Photograph of the Ti Anode after a 3 Razor Shot	29
3.11	Pinhole Exposure of Electron Angular Distribution from the Shot with Feedback and Ti Window	30
3.12	Photograph of the Radial Array Channel Calorimeter	31
3.13	Adsorbed Energy vs Calorimeter Channel Position at the Anode	32
4.1	Machine Drawing of the Cathode Yoke	36
4.2	Photograph of the Modified REBA Diode Assembly	37
4.3	Electron Mapping Package	39
4.4	Electron Pinhole Package	41
4.5	Diode Assembly Drawing	42
4.6	Pinhole and Mapping of Shot 3307 at the Anode	43
4.7	Tube Current and Voltage for Shot 3307	46
4.8	Analysis of the Mapping and Pinhole Results from Shot 3315	47
4.9	Pinhole and Mapping of Shot 3313 at the Anode	49
4.10	Correlation of Prepulse with Beam Quality	52
4.11	Comparison of Display Modes on Pinhole and Map Diagnostics	54

Figures (Continued)

Figure		Page
4.12	Pinhole and Mapping of Shot 3792 at the Anode	56
4.13	Diode and Diagnostic System Arrangement	59
4.14	Pinhole Measurement Near the End of the Inner Cone	60
4.15	Tube Current and Voltage for Shot 3800	63
4.16	Outer Wall Current and Prepulse Voltage for Shot 3800	63
4.17	Net Cone Exit Current	64
4.18	Primary Cone Exit Current	64
4.19	Energy Delivered to the Calorimeter vs. Drift Pressure	66
4.20	Comparison of Triax System Currents with and without Channel Vanes	67
4.21	Proposed Third Version of the REBA Triax	71
5.1	The Hydra Accelerator	74
5.2	Machine Assembly Drawing of the Hydra Diode	76
5.3	Trajectory Control with Chamber Pressure	78
5.4	The Hydra Carbon Pinhole Plate	80
5.5	Pinhole Exposure of Shot 155 at A-K Gap = 0.5 cm Differential Mode	81
5.6	Pinhole Exposure of Shot 155 at A-K Gap = 0.5 cm Quantized Mode	82
5.7	Pinhole Exposure of Shot 322 at A-K Gap = 1.27 cm Differential Mode	84
5.8	Pinhole Exposure of Shot 322 at A-K Gap = 1.27 cm Quantized Mode	85
5.9	Pinhole Measurement of the Electron Angular Distribution at the Cone Exit	87

TRANSMISSION AND COMPRESSION OF AN INTENSE RELATIVISTIC ELECTRON BEAM PRODUCED BY A CONVERGING ANNULAR DIODE WITH RETURN CURRENT FEEDBACK THROUGH THE CATHODE: PART II - THE EXPERIMENTS

CHAPTER I - INTRODUCTION

In Part I of this report, the basic concepts which were used in the design of the converging annular diode with return current feedback (Triax) were reviewed and explained in detail.[1] The explanations and discussions that were made there will only be referred to here when they are needed as guides to understanding the experiments.

In Chapter II of this report, a full discussion is given of the factors which went into the Triax hardware design for the REBA accelerator. The original concepts were developed for higher current machines such as Hydra, but it was felt that much could be learned about the system before Hydra came on line. (Both REBA and Hydra are Sandia Laboratories facilities.) Indeed, most of the results discussed herein were obtained on REBA. Chapter III contains a description of the experiments and a summary of the conclusions reached with the first diode. The diagnostics consisted of diode current and voltage monitors, Faraday cups, calorimeters, witness plates, electron pinhole, and electron intensity distribution measurements.

Chapter IV and Chapter V present the results that were obtained with the second version of the REBA diode and with the Hydra diode, respectively, while the last chapter contains a summary of conclusions, an analysis of the problems encountered with the system, and a discussion of the potential for improvements.

CHAPTER II - THE DESIGN AND FABRICATION OF THE REBA TRIAX

Features of the REBA Accelerator

The REBA facility is composed of a bank of capacitors that are charged in parallel and discharged in series (a Marx generator) to a transmission line which feeds a diode that generates an electron beam. A complete discussion of the machine can be found in a Sandia Laboratories report.[2] A drawing of the diode tube is shown in Fig. 2.1. At the back of the tube within the oil dielectric of the Blumlein are eight spark gap prepulse switches. These switches reduce the voltage across the A-K gap while the line is charging and then break down when the main voltage pulse arrives. The diode shown here has the typical anode and cathode arrangement that had previously been used, but the Triax diode replaced the right end of this tube for these experiments. Even though the impedance of the transmission line is 17 ohms, the Triax diode was generally operated at 5 to 10 ohms. This mismatch and associated reduction in energy output were tolerated in an effort to obtain a higher current of lower energy electrons. With that configuration, the machine generated a peak current of about 140 kA at 1.2 MeV in a pulse that lasted about 100 ns.

The Design of the First REBA Diode

As was pointed out in Part I, if a uniform annular beam can be injected parallel to the channel between two conducting concentric cylinders at $r = \sqrt{r_1 r_2}$, (where r_2 and r_1 are the initial inner and outer cone radii), respectively, then the beam will tend to coast along that line toward the focus without radial oscillations in the average position in the sheet. To first order the location of the focus is independent of the current or electron energy. A return current on the inner cone, driven inductively by the beam, neutralizes the magnetic force which pinches the beam toward the axis and keeps the beam going in a straight line. Current is also returned through the cathode to prevent diode pinch. A sketch of the diode reproduced from Part I of this report is shown in Fig. 2.2.

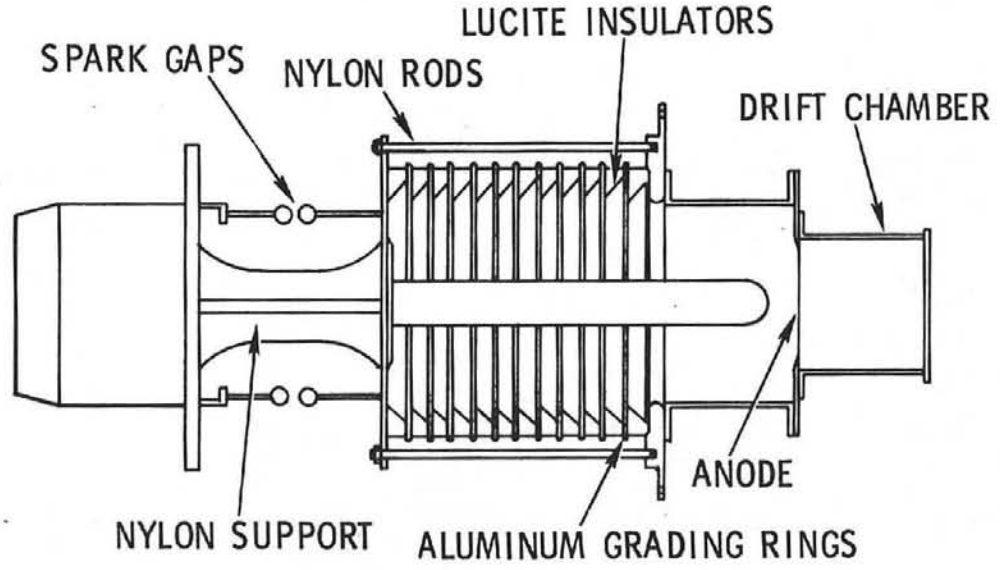

Figure 2.1. REBA Diode with Prepulse Switches

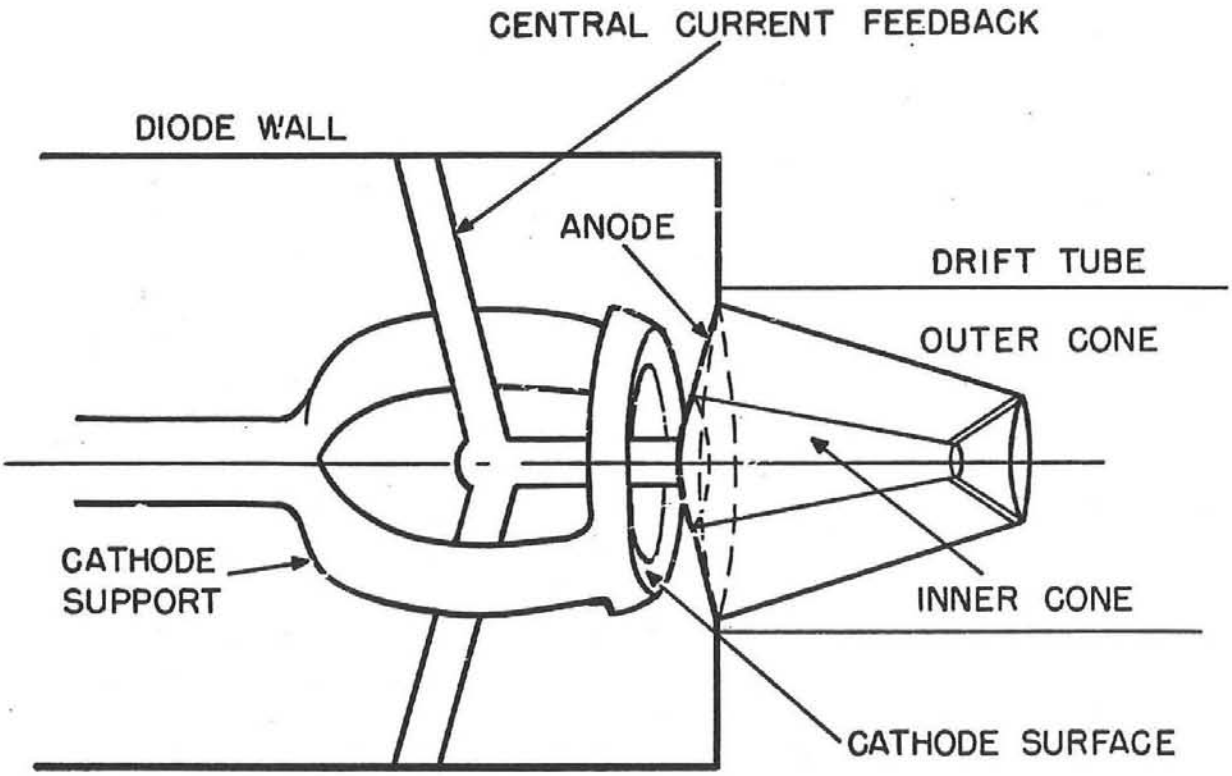

Figure 2.2 Sketch of the Triax and the Transport Cones

We will now review the criteria that determined mechanical design of the first REBA Triax. An assembly drawing is shown in Figure 2.3.

(1) A 20 degree cone angle was chosen because it seemed likely to be the largest angle to which a thin aluminized mylar anode could be stretched. With a six-inch diameter cathode ring, the focal point occurred about six-inches away from the anode. It had been felt that a closer focus would lead to unwanted interaction between the exploding anode and the target. Too large a focus distance would give excessive time for instabilities to grow in the beam before it reached the target.

(2) The approximate six-inch diameter of the cathode was used in order to preserve sufficient separation between conductors in the diode. Even polished metal will begin to field emit seriously with surface electric fields in excess of 200 kV/cm and, therefore, the separation between cathode and ground surfaces had to be maintained at about 5 cm or greater for 1 MV potentials. For higher current situations such as with Hydra, efficient use can be made of magnetic insulation between parallel conductors because electrons emitted are effectively trapped by the magnetic field.

(3) Previous to these experiments, the closest A-K gap which could be used with any reliability was about 2.5 cm. At closer spacings, the beam became erratic and nonuniform. The Triax ring was, therefore, designed with a radial thickness of about 2.5 cm to provide a nominal 20 Ω impedance, according to the 3/2 power law for space charge limited flow.[3] It was hoped that, if ways were found to obtain uniform beams with close A-K gaps, and a narrower ring closer spacing would be possible.

(4) The cathode ring was mounted on a fork so that the axial return current could be fed back to the diode wall by arms at right angles to the fork. The specific dimensions of the fork and feedback arms depended on compromises between the requirements of mechanical strength, minimum electric fields on the cathode surfaces, and proper inductances in the current

NOTE:
▷ ONLY ONE OF ITEMS 10, 11, & 12 IS USED AT A TIME.

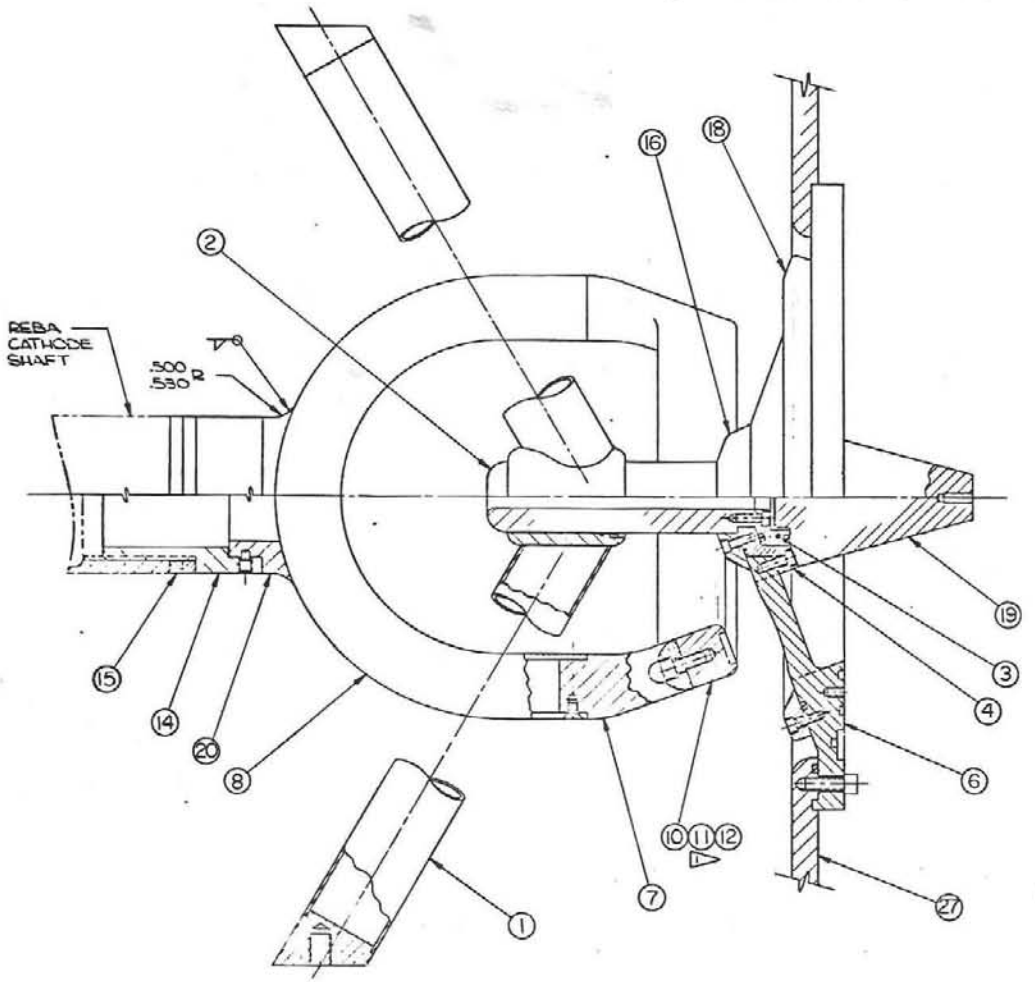

3		SCREW, SET, FULL DOG, 1/4-20 × 1/4 L			34
12		SCREW, MACH, SOC HD 1/4-20 × 3/4 L			33
4		SCREW, MACH, SOC HD 1/4-20 × 3/8 L			32
8		SCREW, MACH, FLAT HD, 10-24 × 1/4 L			31
16		SCREW, MACH, SOC HD, 8-32 × 1/2 L			30
4		SCREW, MACH, SOC HD, 6-32 × 3/8 L			29
					28
1		ALUM. ALLOY 6061-T6		9	27
					26
AR		CONTACTS, FINGER		7	25
2		TUBE, BRASS YELLOW, FREE MACH		8	24
1		BRASS, YELLOW FREE MACH		8	23
2		BRASS, YELLOW, FREE MACH		8	22
					21
1		ALUM. ALLOY 6061-T6		8	20
1		ALUM. ALLOY 6061-T6		2	19
1		ALUM. ALLOY 6061-T6		6	18
					17
1		ALUM. ALLOY 6061-T6		6	16
2		CRES STEEL, TYPE 304		6	15
1		CRES STEEL, TYPE 304		6	14
					13
1		BRASS, YELLOW FREE MACH	1	5	12
1		BRASS, YELLOW, FREE MACH	1	5	11
1		BRASS, YELLOW, FREE MACH	1	5	10
					9
1		TUB. ALUM, 6061-T6 OVAL 3×1 g .125 WALL		4	8
2		ALUM. ALLOY 6061-T6		4	7
1		CRES STEEL, TYPE 304		3	6
					5
1		NYLON		2	4
1		ALUM. ALLOY 6061-T6		2	3
1		ALUM. ALLOY 6061-T6		2	2
1		WELDMENT		7	1

Figure 2.3 Machine Drawing of the Triax Diode

circuits. For example, if the axial conductor were too small, its inductance would prevent an adequate return current from flowing there and the beam would pinch in the diode. On the other hand, for too large a conductor the cathode would emit toward the feedback system rather than toward the anode. Furthermore, magnetic insulation would not develop on the axis between the end of the axial return current bar and the base of the cathode fork.

(5) The inner structure of the anode was supported by four thin ribs that passed across the drift region just outside the window. In this way, the ribs did not disturb the azimuthal symmetry inside the diode. Normally a 0.001 cm aluminized Mylar window was taped onto the outer retaining ring and then stretched over the anode cone. After the axial conductors had been assembled on the anode plate, the assembly was pushed into the diode so that the axial stub slipped into the feedback bar sleeve.

(6) The cone channel was made 5 cm wide so that diagnosis of the beams would be easier.

(7) Because the cathode-anode alignment is important here, the base of the cathode shank was mounted on a plate-and-ball arrangement so that the shank angle could be controlled by bolts that could be reached through the anode opening. Alignment could then be maintained easily to within 0.05 cm.

Cathode Emitters

Although many studies of cathode emitting surfaces have been conducted by all of the groups using high-current electron beams,[4,5,6] experiments usually reveal that for each machine and each diode there are particular cathode types which work best. We therefore also undertook such an investigation for this geometry and tried three basic types of cathodes, epoxy-filled grooves (plasma cathode), carbon emitters, and sharp edged emitters.

The first three cathode types tried are shown in Fig. 2.4. All of them generated beams of comparable uniformity, but the razor cathodes were not very practical because about 100 razors had to be replaced after each shot. The epoxy-ring cathode was superior in uniformity, and it only had to be sanded off and polished after each shot.

Another practical difficulty with this conical diode geometry is that changing the A-K gap was not just a matter of moving the cathode forward or backward. If the gap change was to be more than just a few millimeters, then a a whole new cathode ring had to be fabricated to maintain the proper radial position of the emitter. Of course, this would cause no problem once the A-K gap was fixed.

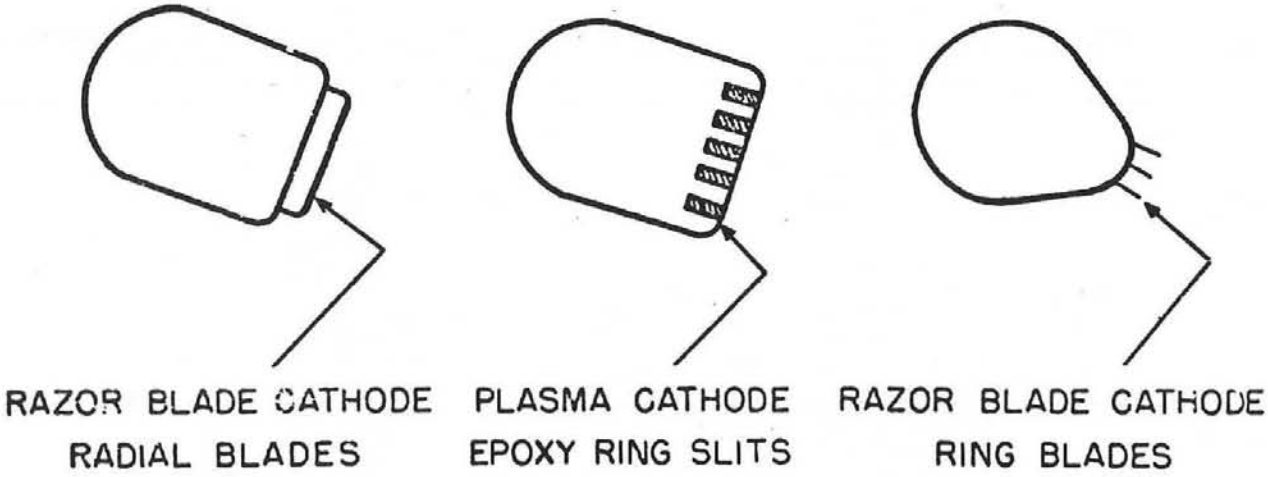

Figure 2.4 Cross Section of Ring Cathode Emitters

CHAPTER III - TESTS WITH THE ORIGINAL TRIAX DESIGN

The initial steps were directed towards fundamental questions about the system such as the following: can a uniform annular beam be formed, is the feedback of current through the cathode really needed, does the beam pass through the anode without just jumping to the inner structure, and does the cone channel actually guide the beam.

Tests Without the Feedback System

The diode without the feedback arms was first fired between the cones within which thin pieces of cinemoid had been mounted in the (r,z) plane as shown in Fig. 3.1. Figures 3.1 and 3.2 show that the beam pinched inward and spalled the inner cone. Obviously, the feedback through the cathode is necessary. The spall marks and the Cinemoid damage both show that the beam was azimuthally nonuniform and became concentrated into two beams oriented at right angles to the fork by the time it struck the inner cone.

On a second shot, four 0.318 cm thick copper plates with 0.318 cm diameter holes were placed just beyond the anode. Pieces of rose cinemoid 1.27 cm beyond this pinhole plate gave a measure of the electron directions and angular distributions. Figure 3.3 shows those plates from the diode side in place between the anode support ribs after the window had been burned away by the electron beam pulse. The electron pinhole diagnostics are described in more detail in other Sandia reports.[7,8,1]

An image quantizer reading of one Cinemoid quadrant is reproduced in Fig. 3.4. The spots are almost as narrow as the holes but move inward as the beam pinches during the pulse. It is extremely unlikely that these streaks are steady-state, angular distribution patterns. Other pinhole data later in the report will give stronger evidence that those streaks are formed by a moving spot (as a narrow distribution of electrons changes direction). Notice also that the streaks are not really radial, but instead angle sideways as the beam pinches.

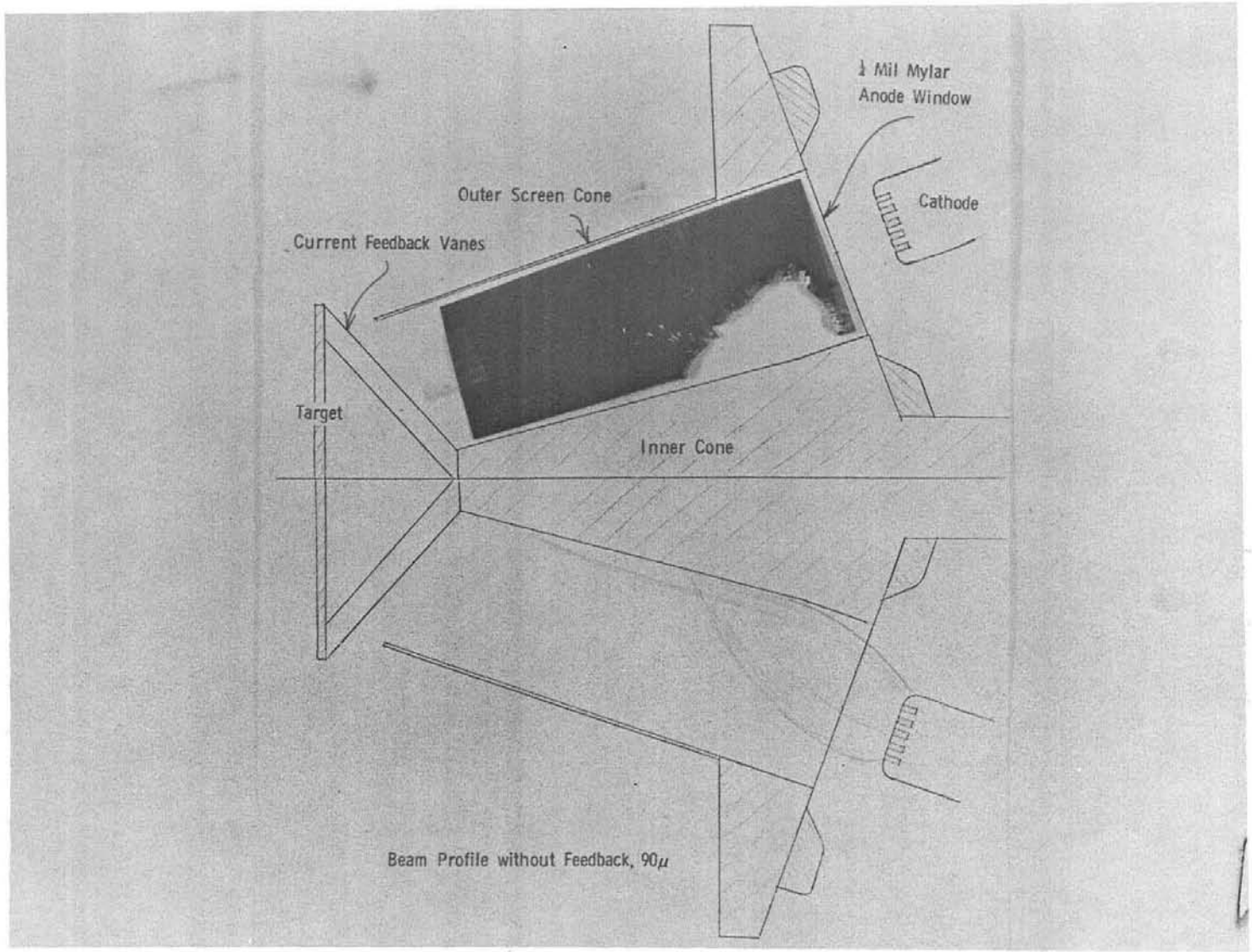

Figure 3.1 Photograph of Inner Cone Spall Marks

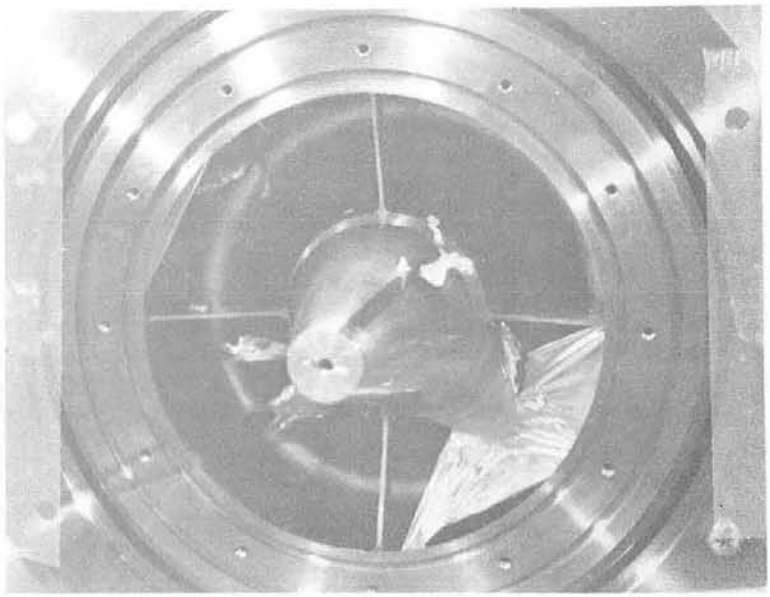

Figure 3.2 Beam Profile without Feedback, 90μ

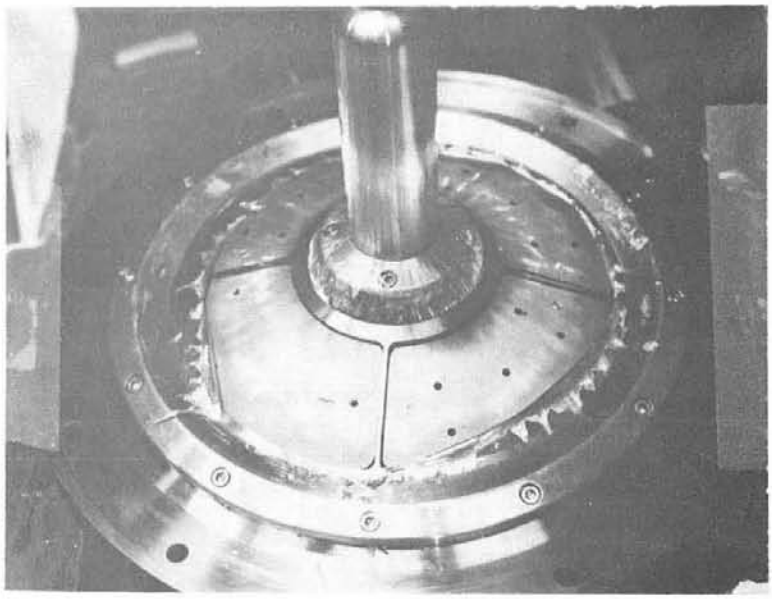

Figure 3.3 Photograph of Pinhole Plates after a Shot

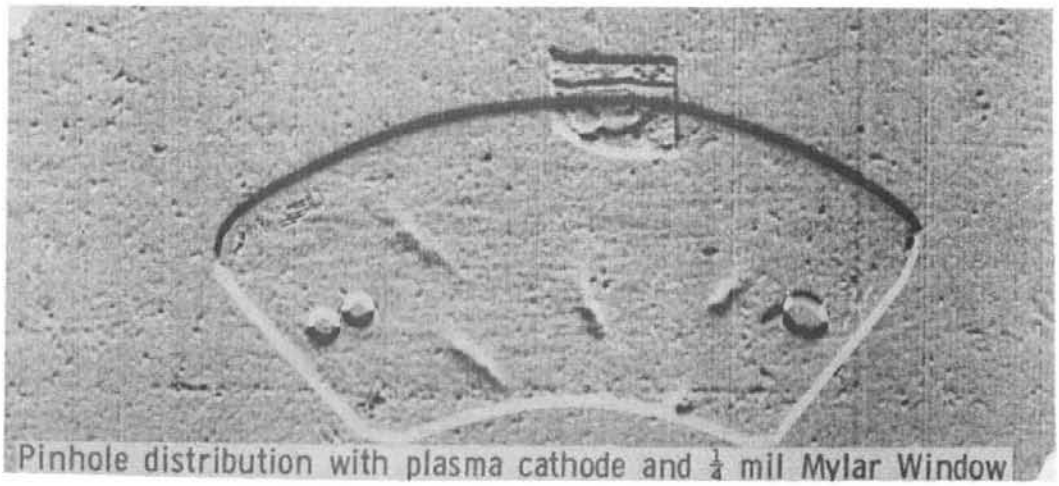

Figure 3.4 Pinhole Exposure of Electron Angular Distribution from the Shot without Feedback

There is a simple explanation for this motion that will be discussed in the next section, but its cause was not immediately recognized. Analysis of the exposure distribution across the narrow portion of the streaks indicated an average spread of only about 5 degrees FWHM. This was very encouraging at the time because, if only initial angular momentum is considered, it implies the possibility of focusing the beam down from an area of about 60 cm^2 to 3 cm^2.

There was evidence from open shutter photographs of the diode during the shot that a portion of some beam leaped across to the axial conductor from the base of the cathode fork. The fork was subsequently lengthened by 717 cm. On this second shot the A-K gap was 1.9 cm, the peak tube voltage was 1 MV, and the total diode peak current was 150 KA.

First Tests of the Triax System

The addition of the feedback bars made a striking difference in the character of the beam. Substantially all of the beam now entered the cone channel and for a considerable distance was guided between the walls. The burn pattern in another (r,z) plane plastic is shown in Fig. 3.5. The radial nodes that should appear in the sheet are clearly visible early in the channel, but they become washed out further down. Notice also that the beam enters the channel at too large a radius and therefore is pushed inward by the outer wall. The beam then oscillates in the channel until it drifts outward. Here we have the first evidence of a serious angular momentum problem in the beam. As was discussed in Part I of this report, if the electrons begin with large azimuthal velocities or acquire them in the channel, the conservation of angular momentum implies that they cannot reach the axis and, in fact, will be separated radially according to angular momentum as they attempt to approach it. A witness plate at the end of the cones showed that again the beam had broken up into two bunches that were oriented at right angles to the plane of the fork. There was no correlation with the position of these beams with the orientation of the anode ribs.

The A-K gap in this case was only 1.59 cm, but the cathode ring had been designed for a 2.5 cm gap. This is the principal reason that the beam entered at too large of a radius and was forced to oscillate

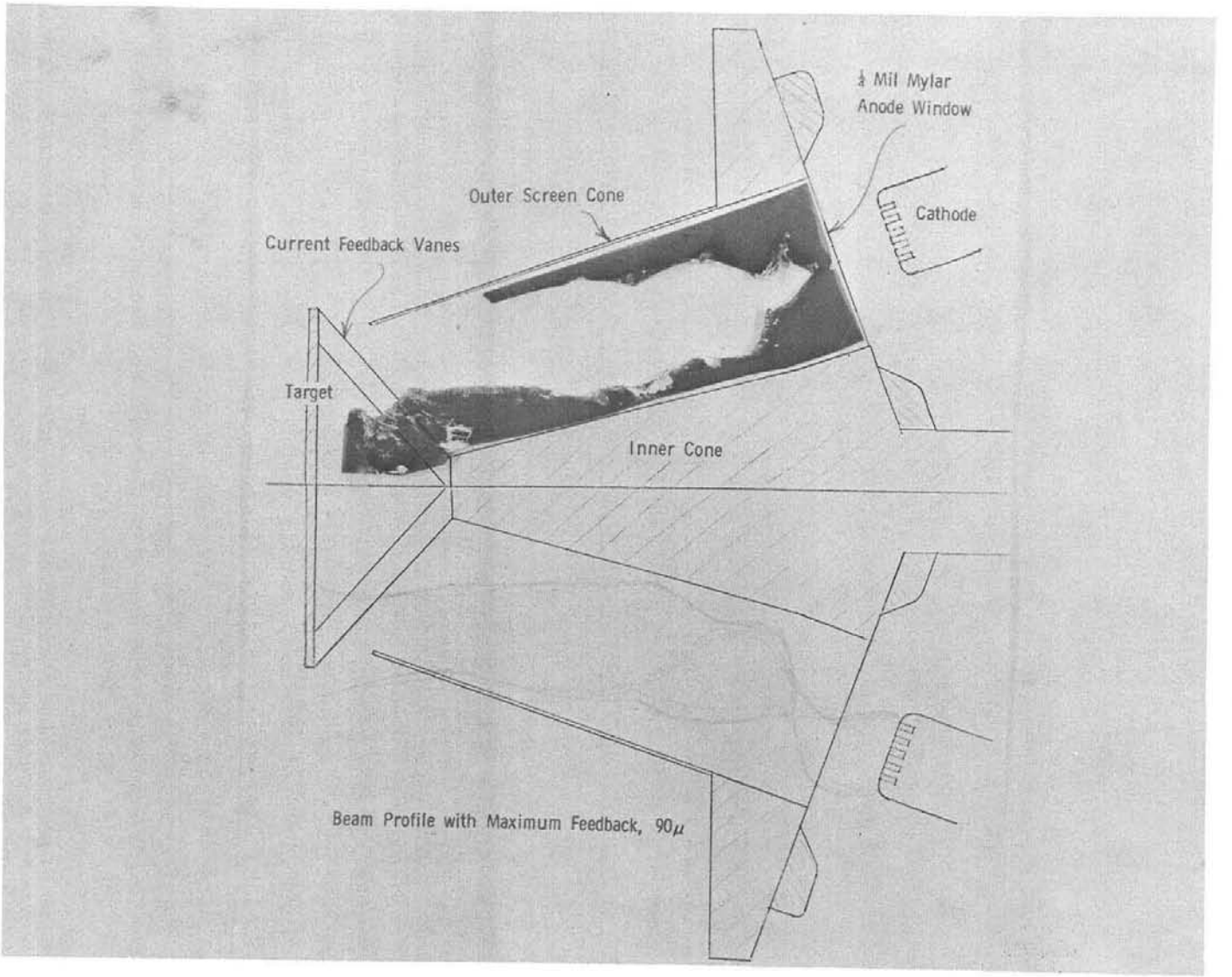

Figure 3.5 Beam Profile with Maximum Feedback, 90 μ

in the channel. In this configuration a resistive current monitor, mounted in the outer diode wall in front of the feedback arms, measured 63 kA peak current while one behind measured 125 kA so that indeed a current of approximately 1/2 must have been flowing on each of the inner and outer current paths as the triaxial theory predicted would happen. The drift channel pressure was .090 Torr in this case so that the high net current in the channel generated a strong B field and produced the closely spaced nodes.

A series of tests was conducted to see if the razor blade cathodes discussed in Chapter II would provide better uniformity. (A photograph of the radial razor cathode is shown in Fig. 3.6.) The conclusion was that the epoxy ring type was slightly better.

At the same time, a new cathode ring was designed for a 1.59 cm A-K gap that would hold three circular razor bands at 0.635 cm spacings from which beams would be launched at the proper radius. This new razor cathode ring is illustrated in cross section in Fig. 3.7. The burned path in the plastic clearly showed that, with injection at the proper radius, the beam started straight down the channel with no radial oscillation. At 3 Torr pressure, where there is high current neutralization, the distance between nodes was greatly increased. The azimuthal symmetry improved considerably and part of the beam pinched off the end of the cone, but the outer boundary still spread toward the outer wall. We finally realized what was happening to cause the beam concentrations at 90 degrees from the cathode fork. The situation is illustrated in Fig. 3.8. The cathode ring was fairly narrow in the Z-direction and, after the current from the fork reached the ring, it flowed up along the ring and generated a magnetic field around it. Electrons coming off the cathode surface were turned by this field toward the azimuth which is 90 degrees from the fork. As a consequence the beam was concentrated at two points out beyond the anode. Obviously this field could be eliminated by making the current flow to the emitting surface from behind rather than along the ring. As is shown in Fig. 3.9 copper pieces were taped into the corners. With this asymmetry was reduced.

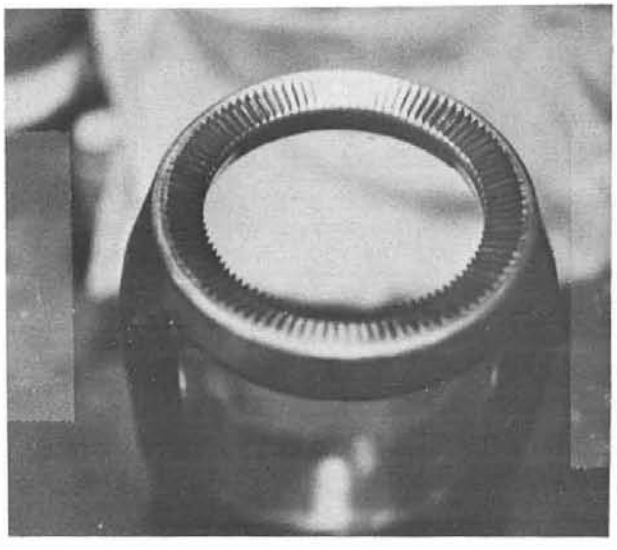

Figure 3.6 Photograph of the Radial Razor Cathode Ring

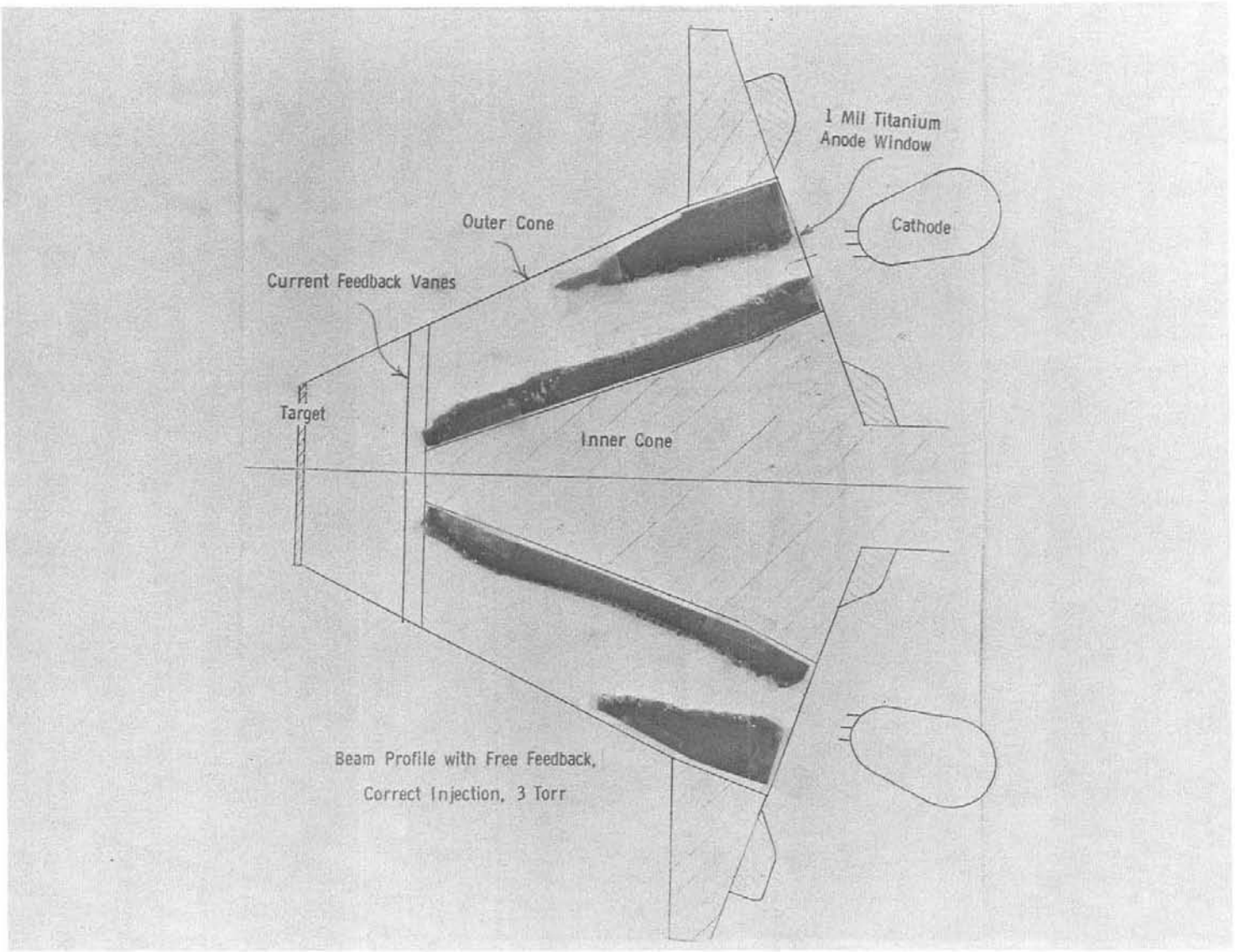

Figure 3.7 Beam Profile with Feedback, Correct Injection, 3 Torr

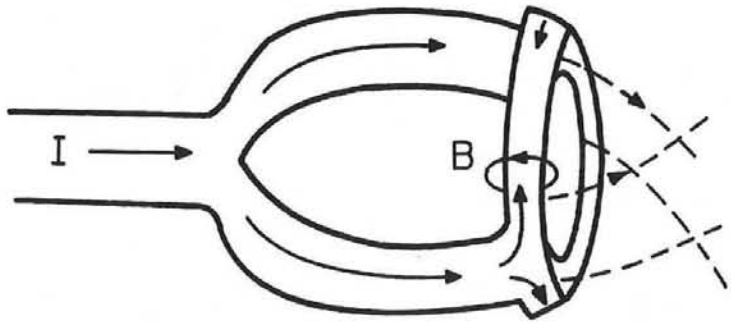

Figure 3.8 Turning of Electrons in the Cathode Ring B Field

Figure 3.9 Photograph of the Cathode Shank with Copper Filled Corners

Some additional illustrations will provide a more complete picture of what the beam looked like at the end of this first series of tests. Figure 3.10 is a photograph of a 0.0025 cm titanium window after it was used with the 3-hoop razor cathode. The bright areas are the places where oxidized material was cleaned off and where metal was deposited. The two damaged rings are the overlap regions of the 3 razors. One can see that on opposite sides the beam had started to concentrate at these 90 degree points.

Actually this 1 mil titanium window is unsuitable if a good focus is ever to be obtained because the average multiple scattering angle for 1 meV electrons is about 20 degrees in this material. This scattering introduces too much angular momentum into the beam. An image quantizer reading of another pinhole exposure (in Fig. 3.11) reveals very broad, shallow distributions from each pinhole. This pinhole measurement was taken with the feedback system in place and there is no evidence of any radial spot motion.

Before these investigations began, a short radial array of 0.635 cm^2 carbon calorimeters was fabricated so that the radial distribution of energy in the channel could be examined. The device is pictured in Fig. 3.12 and a graph of the energy deposited versus radial position is shown in Fig. 3.13. The array had been designed for measurements on down the channel, but was only used near the anode.

With this first diode configuration a measurement was made of the energy distribution at the exit of a cone with a planar array of carbon calorimeters. The cone geometry was the same as that shown in Fig. 3.7 except that the outer cone was cut off so that it had a 7.5 cm diameter exit which was 1.27 cm beyond the end of the inner cone. This was the z-position where the computer program predicted the focus to occur if there were no angular momentum in the beam. The conditions were the following: a 3-razor hoop cathode, A-K gap of 1.27 cm, drift pressure of 3 Torr, and 0.00063 cm aluminized Mylar anode. Indeed, most of the energy (about 1500 cal) made it to the end of the cone, but it certainly was not focused well. The beam in fact was a hollow

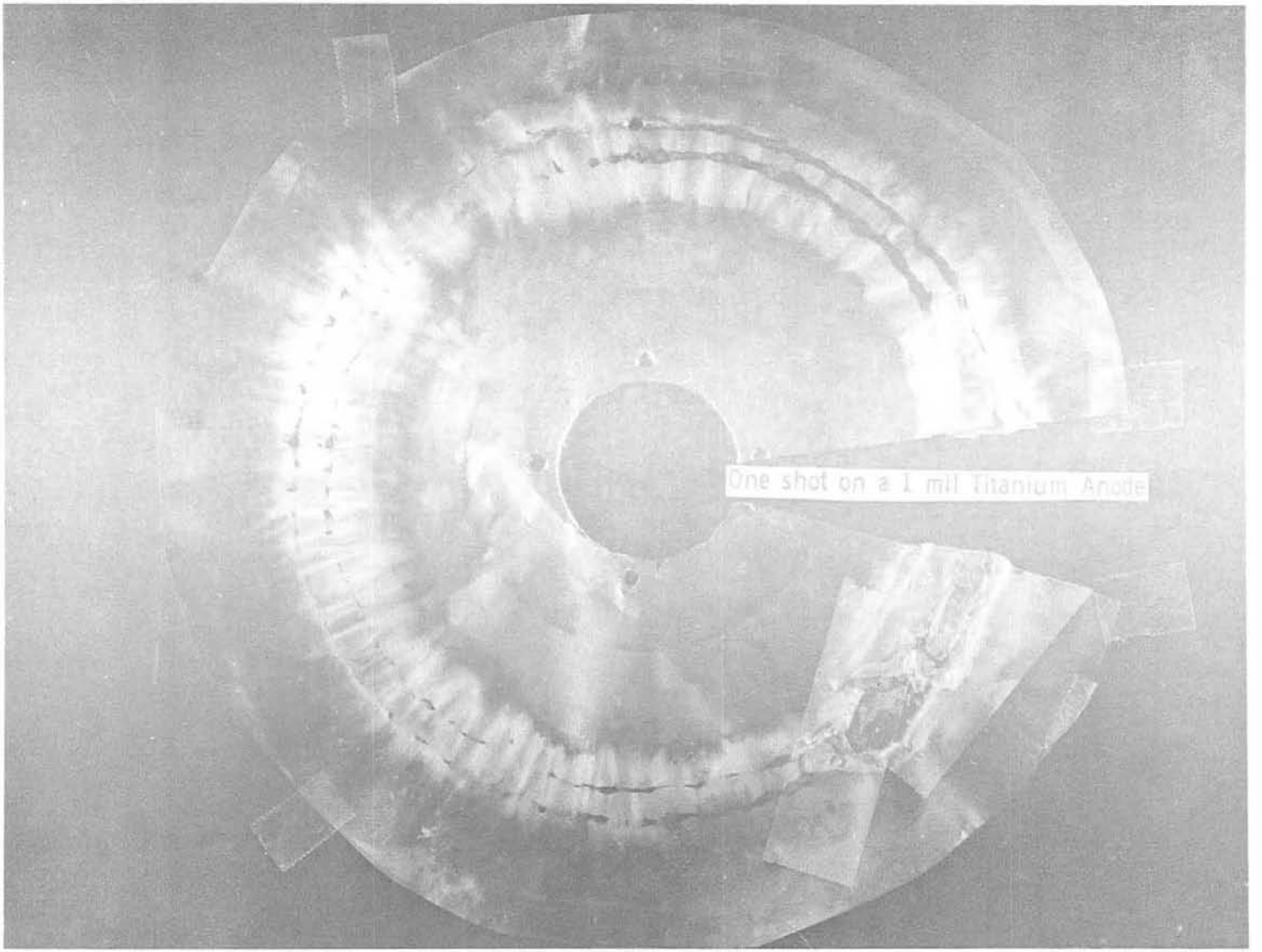

Figure 3.10 Photograph of the Ti Anode after a 3 Razor Shot

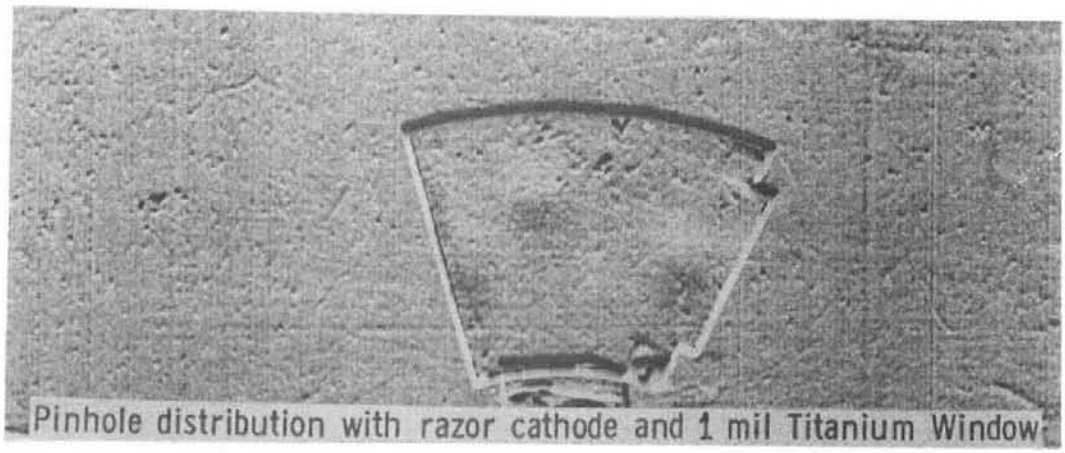

Figure 3.11 Pinhole Exposure of Electron Angular Distribution from the Shot with Feedback and Ti Window

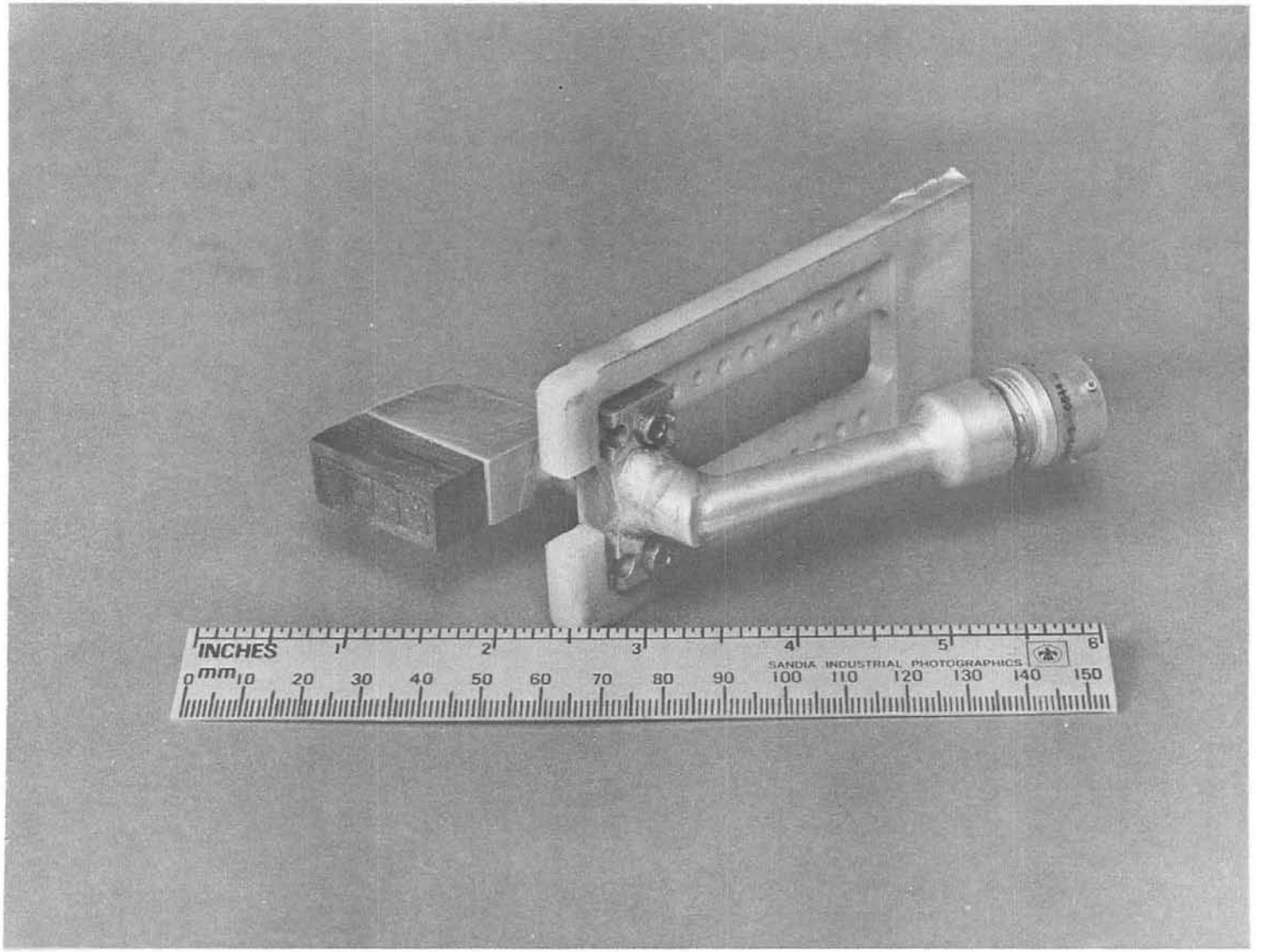

Figure 3.12 Photograph of the Radial Array Channel Calorimeter

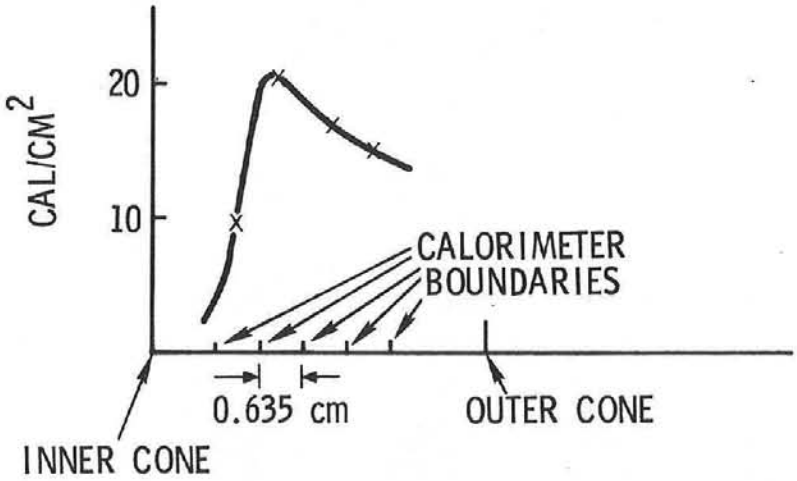

Figure 3.13 Adsorbed Energy vs Calorimeter Channel Position at the Anode

doughnut peaked at the outer edge to about 40 cal/cm^2 compared to 20 cal/cm^2 at the anode. Thus, only a factor of two in intensity had been gained and the energy was deposited into an annulus.

Finally, it should be pointed out that the shots that have been discussed here in detail were actually the best that had been obtained. Quite often, especially with the closer A-K gaps, the shots were extremely nonuniform. For example, the beam might leap all in one filament to the anode retaining ring or to a supporting rib. In those cases the current and voltage measurements indicated that the diode was shorted. Careful alignment helped, but the main problem was associated with prepulse. The prepulse problem will be discussed thoroughly in the next chapter.

Summary and Conclusions about the First Triax Diode

Some of the more important conclusions about the first Triax diode experiments are the following.

(1) The triaxial beam theory is confirmed. If the beam was injected at the wrong radius, the sheet oscillated within the channel; when it was injected parallel to the channel at $r_0 = \sqrt{r_1 r_2}$ it traveled straight down towards the focal point until the influence of the angular momentum began to dominate. If all of the current was fed back to the inner structure, the beam expanded initially.

(2) The angular momentum in the beam did prevent good focusing. It can be present for a number of reasons including the following: (a) azimuthal asymmetry in the diode caused mainly by the B field generated by currents flowing along the cathode ring, (b) initial angular distribution of the electrons as they are emitted from the cathode, (c) scattering in the anode foil, (d) instabilities in the diode or drift chamber and (e) interaction of the beam with the anode support ribs.

(3) Oscillations in the beam sheet thickness were seen, and as expected their spatial frequency depended on the drift tube pressure which controled the net current. One could presumably measure that nodal wavelength and use the program of Part I to find a net beam current in the channel, but there would have been nothing to compare

it with because the inner and outer wall currents in the drift region were not being measured.

(4) Careful alignment was necessary, but small misalignments could not account for the extremely erratic shots that often occurred. Diode shorting usually took place quite early in these erratic shots, indicating that a highly conducting plasma had closed the gap.

(5) The razor blade and the epoxy ring cathodes produced comparable beams, but the epoxy-ring type was easier to use and to recondition.

In the next chapter, the second Triax diode will be discussed. It was unfortunate that the necessary changes in the geometry of the system were difficult to make. However, after they had been made very great improvements in beam quality appeared immediately.

CHAPTER IV - THE MODIFIED REBA TRIAX DIODE

It is fairly obvious from the results of the last chapter that the symmetry in the diode and also the documentation of the character of the beam (versus diode parameters) as it emerged from the anode had to be improved before the basic focusing properties of the Triax concept could be tested and their practical limits could be found. The principal design changes made will be discussed first and then the additional experiments. Improvements in the diagnostics were also made and used for determination of the beam parameters.

Modifications of the REBA Triax

A major change was made in the cathode support structure. The main objective was to find a way to feed current to the cathode ring uniformly from behind and, at the same time, maintain the ability to feed return current through the ring. The geometry was too complicated for detailed calculations to be very useful, so that simple estimates and physical intuition had to be used. A machine drawing of the yoke is shown in Fig. 4.1. The yoke was made azimuthally symmetrical back 7.5 cm from the brass cathode ring emitting surface. Each ring slid with a snug fit onto the yoke. It could be quickly removed for reconditioning. In this way no bolt heads or edges of countersunk holes were present that could cause nonuniform emission. (Pictures had revealed such edge emission in the old configuration.) From the shank the current was fed to the yoke arms and then gradually to the cylindrically symmetric portion of the support. The whole structure was cast in aluminum, machined partly by hand and polished. A photograph of the diode assembly is shown in Fig. 4.2. One can see that the fork length was increased further. In the base of the fork where the field is low, a bolt head that controls the linear shank adjuster was positioned. By reaching through the cathode one could turn a bolt and adjust the A-K gap.

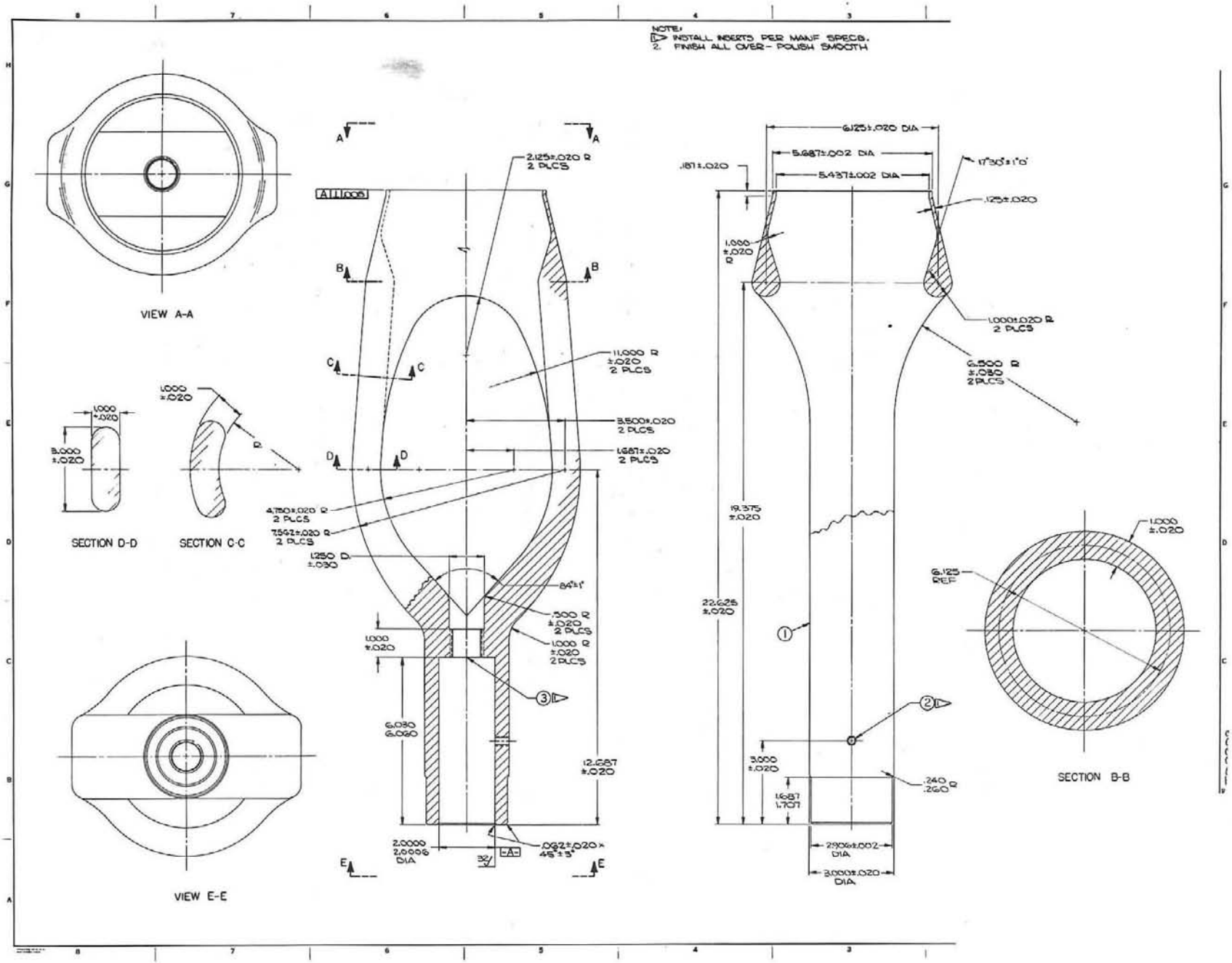

Figure 4.1 Machine Drawing of the Cathode Yoke

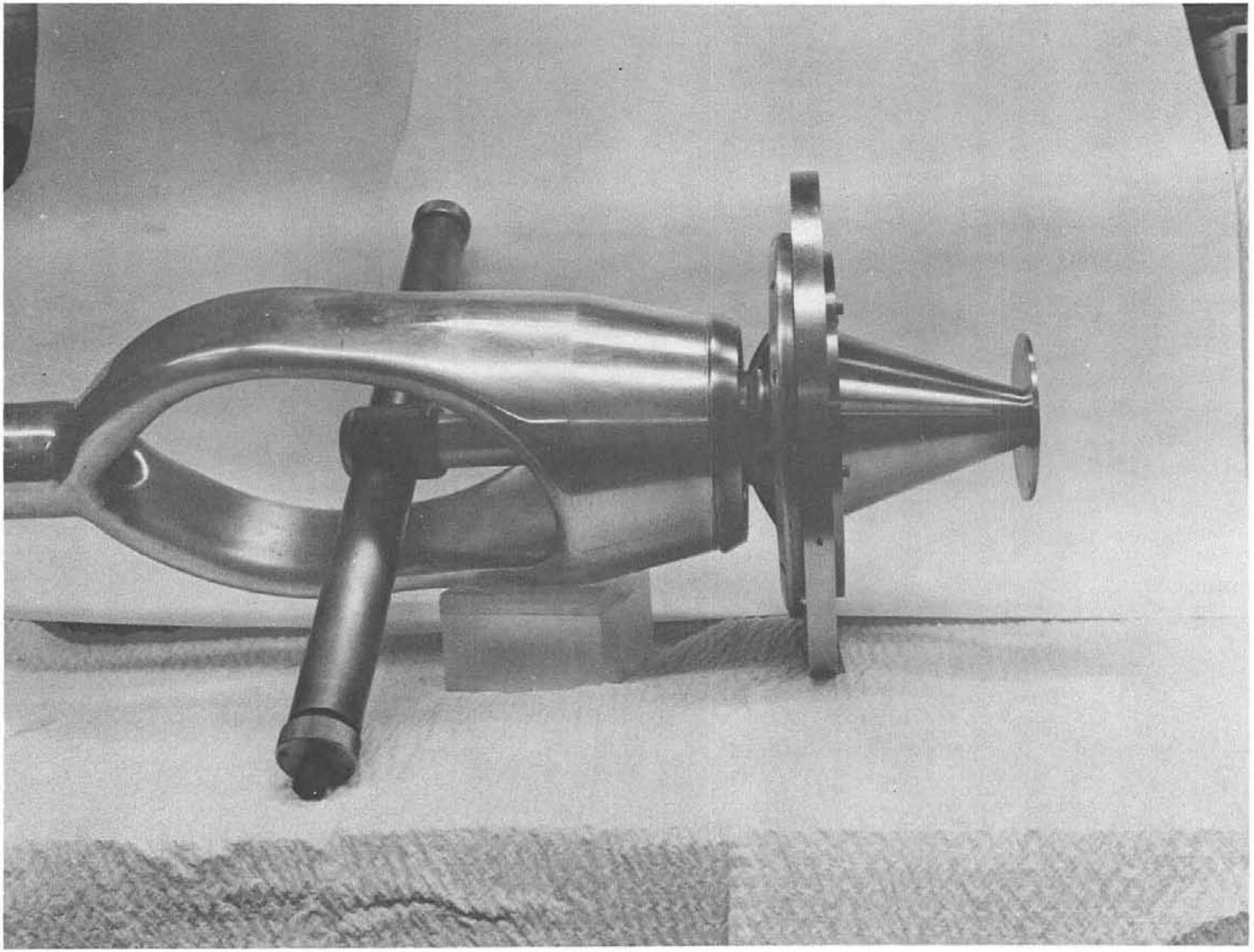

Figure 4.2 Photograph of the Modified REBA Diode Assembly

The axial feedback shaft was hollow and was designed so that cables from a monitor could be fed all the way from the tip of the inner cone out through the feedback bars. A typical monitor might be a Rogowski coil mounted within the inner cone that would read the inner cone current. In this Triaxial geometry the wall currents on both the inner and outer conductors have to be monitored before the net current in the beam can be found, and these currents can be very different from those in the diode. We found that the improved mechanical design reduced the turnaround time between shots by about a factor of three.

The objectives of the next series of experiments were the following.

(1) Fully develop the electron mapping and pinhole technique for this system.[7] This was because the injection parameters of the beam into the channel are so important for this geometry.

(2) Measure the beam properties, particularly uniformity, of the new cathode.

(3) Test new cathode shapes and emitting surfaces to find one which provides a narrow beam that is traveling most nearly parallel to the channel at the anode.

(5) Measure the focusing properties of the best available beam.

Electron Pinhole and Mapping Diagnostics

Just beyond the anode window, eight thin titanium plates were mounted. They each were shaped to fill the channel and to cccupy a 45 degree sector of the annulus. In general four of the plates were of varying thickness from 0.0127 cm to 0.0508 cm. Just behind them were 0.005 cm thick sheets of 4-chlorostyrene packaged in black filler paper.[9] (4-chlorostyrene is a plastic which turns green with an optical density that is proportional to the dose delivered to it.) The configuration is shown in Figure 4.3. The titanium attenuator blocks out low-energy electrons and attenuates the rest of the beam so that only a fraction can penetrate through and expose the plastic.

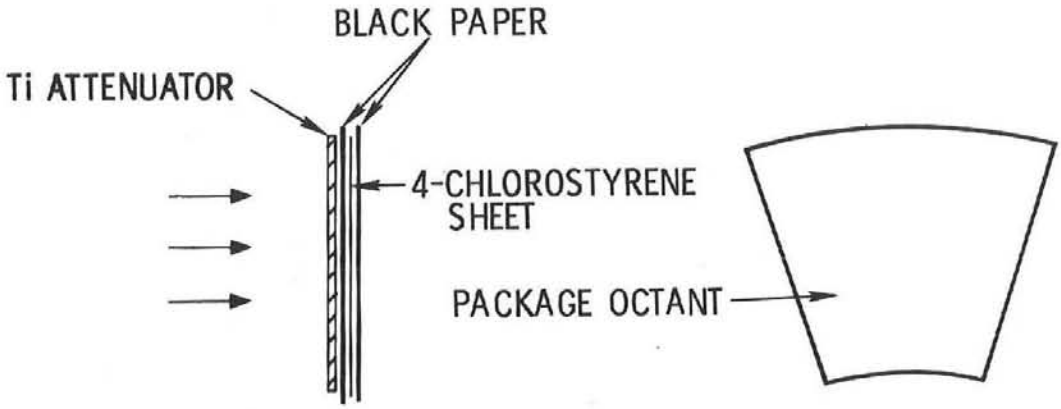

Figure 4.3 Electron Mapping Package

Because the attenuator is thin and the electrons usually have energies of 1 MeV or less, those that penetrate cannot have moved far laterally in the plate. Therefore they emerge within a small fraction of a millimeter of the position they enter the plate (despite the multiple scattering) and the spatial resolution is very high. Thus, the exposure versus position is almost linearly proportional to the beam intensity on the plate, and it provides an excellent map of the integrated current density distribution at the attenuator plane.

The other four plates are usually thicker than an electron range. A typical one was 0.0635 cm thick and had radial arrays of holes drilled into it as shown in Fig. 4.4. Again a black paper and 4-chlorostyrene package was mounted behind, but in this case it was positioned at some appropriate distance (e.g., 0.635 cm) behind the plate. As has been mentioned before, this system provides measurements of the angular distribution of the electrons at various positions in space. What is really surprising is that, even though this is a completely time-integrated measurement, it provides a great deal of information about the time history of the beam.

The Investigations of the Triax Diode Output

The first of the new cathodes is shown in position in Fig. 4.5 in full-scale. It was a brass ring with six narrow grooves filled with epoxy. We hoped to achieve a narrower beam with higher initial current density than with the old epoxy ring by using a narrow ring with a smaller 1.59 cm A-K gap. The emitting surface was convex because the first tests showed that the beam was converging at the anode, and our goal was to obtain a parallel beam there if possible.

The 4-chlorostyrene sheets that were exposed on the second shot are shown in Fig. 4.6. This is an image quantizer contour map of each of the octant sections. Each shading change indicates a new contour interval. The most obvious point is that the gross structure shows a high degree of azimuthal symmetry and there is no correlation between the position of the fork arms and any structure in the pinhole spots or the intensity maps. The new cathode yoke worked even

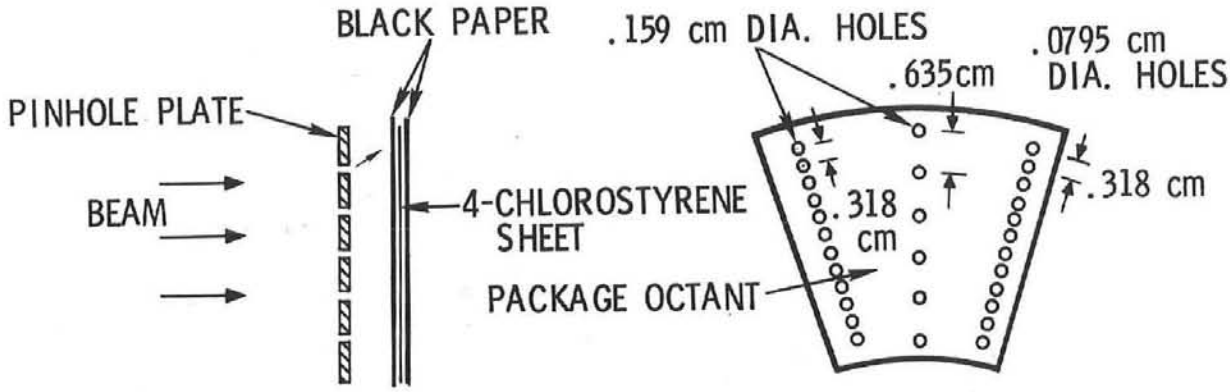

Figure 4.4 Electron Pinhole Package

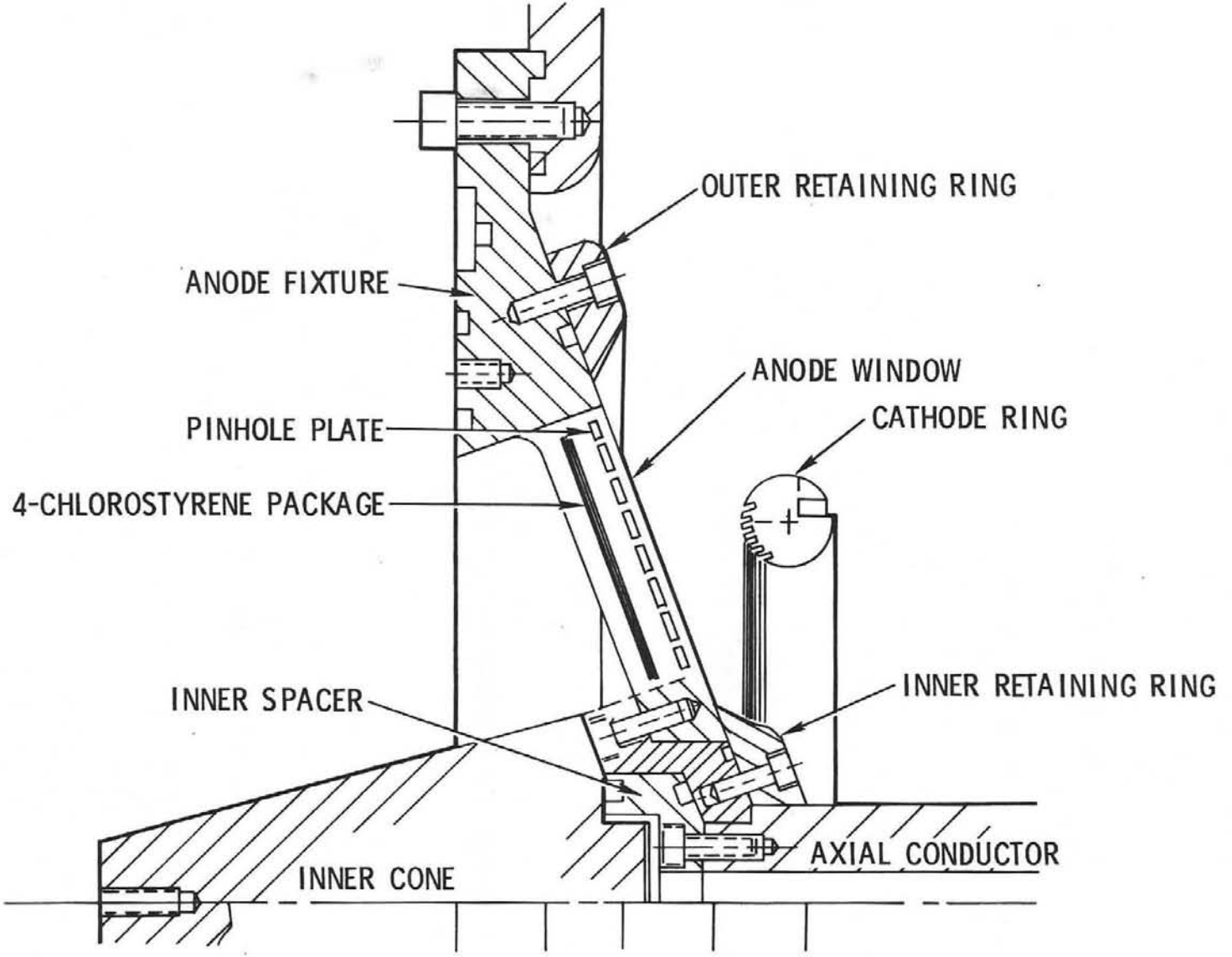

Figure 4.5 Diode Assembly Drawing

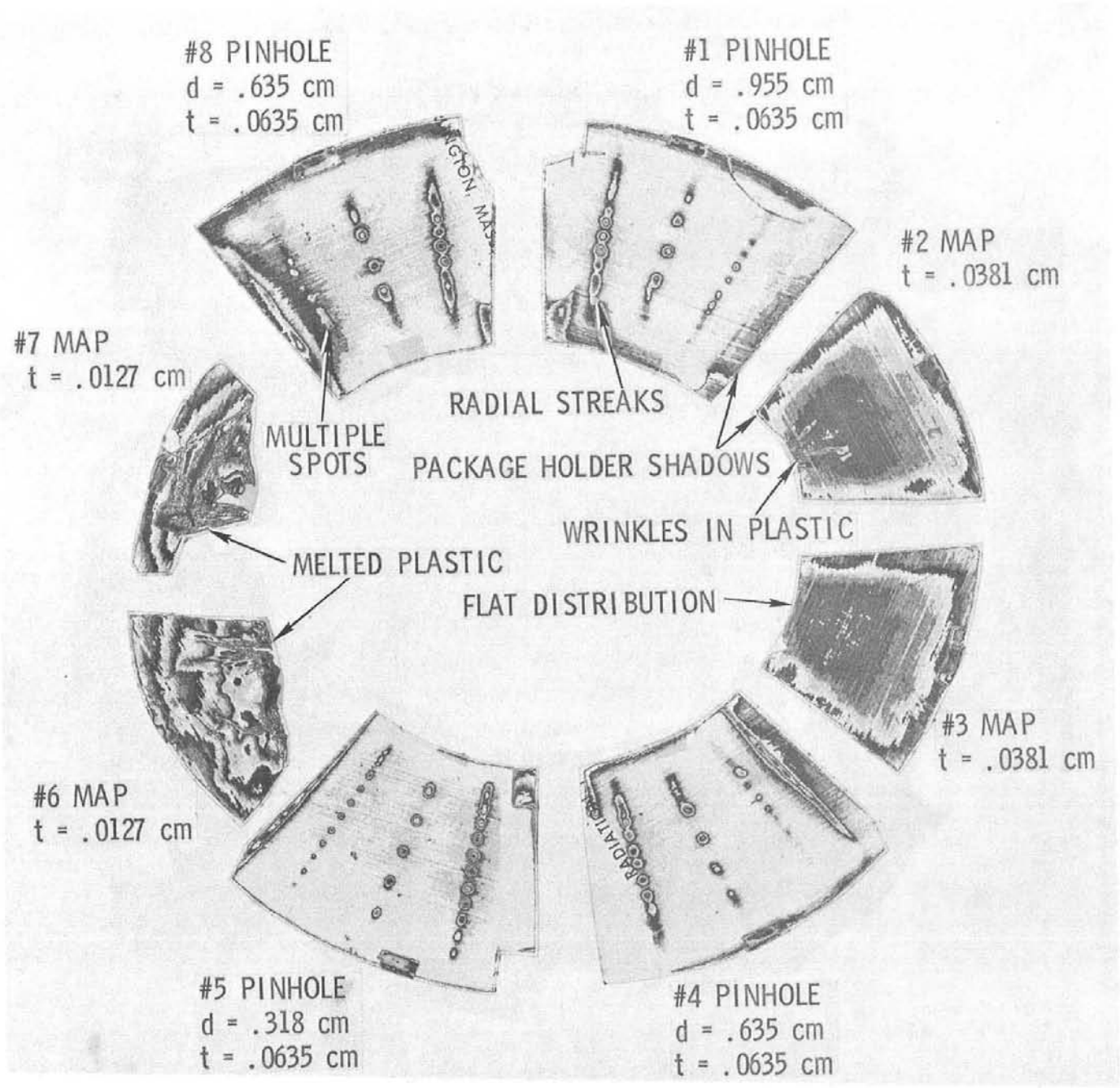

d = PINHOLE PLATE TO DOSIMETER SEPARATION
t = ATTENUATOR OR PINHOLE PLATE THICKNESS

Figure 4.6 Pinhole and Mapping of Shot 3307 at the Anode

better than had been anticipated in this respect. The most effective way to discuss this measurement is to consider individual octants.

#1. The beam spots move mostly radially as is necessary for a good quality beam. Two other important features are the following: first, the spots are almost the same size as the holes indicating that the electrons at a given position have a very narrow angular distribution (about 5 degree); second, the spots pinch toward a central radius that corresponds to $r_o = \sqrt{r_1 r_2}$. Even though the cathode was convex this time, the sheet is still converging late in the pulse as it emerges from the anode.

#2. This map shows the most uniform spatial distribution that has yet been obtained on any shot. There is just a very slight splotchiness. We will later show maps with much more structure. One unfortunate feature is that the beam is quite thick radially. The boundary cannot be seen and the beam is at least 3 cm thick.

#3. This map exhibits the same characteristics as #2. The faint lighter border is shadowing from the attenuator bracket.

#4. This is much the same as #1, but there may be slightly more sideways spot motion. This is certainly a small scale, almost random motion.

#5. The closer dosimeter package spacing here allows us to resolve most of the spots and the slight pinching can still be seen.

#6. The 0.0127 cm attenuator was just too thin and the plastic was partly melted. However, near the outer edge there is a little evidence of a weak striated structure.

#7. Similar to #6 but the damage is even worse.

#8. Similar to #4, but here one of the smaller spots indicates more than one source may contribute to it (multiple spots). Multiple spots are difficult to see in these contour maps but can be clearly seen when the dosimeter is observed with the naked eye. (A photograph of another pinhole and map exposure with multiple spots is shown later in Fig. 4.11.)

The beam parameters for this shot were the following: A-K gap = 1.27 cm, drift tube pressure = 1 Torr, Marx charging voltage = 65 kV, and anode window = 0.000635 cm thick aluminized Mylar. The current and voltage traces are reproduced in Fig. 4.7. In each trace is a fiducial mark so that accurate time correlation between the traces can be made. The higher frequency oscillation is real signal on both monitors.

The current was measured by a resistive current monitor behind the feedback bars. The resistive voltage monitor, however, is located at the base of the tube and therefore its signal contains a contribution from the tube inductance. When that tube inductance contribution is subtracted out, the peak cathode tip voltage comes out to be only about 1.1 MV. One feature that is evident here is that the current continues to rise almost to the end of the voltage pulse indicating a fall in impedance starting from about 9 ohms and decreasing to about 5 ohms just before it drops to zero. This change in impedance during the pulse can be ascribed to plasma closure of the diode gap at a rate of between about 2 to 8 cm/μsec.

A more careful analysis was made of pinhole results from another shot which had identical parameters as 3307 above except that the cathode ring was narrower. A magnified drawing of the tip and the anode is shown in Fig. 4.8. At the anode plane, the locations of the pinholes are numbered and, from the center of each pinhole, a line is drawn through the average maximum displacement (at maximum sheet pinch) of the exposed spots on the 4-chlorostyrene. At the top right the angles that these rays make with the cone angle (20 degree) are listed. The pinhole spot 11 was extremely weak and that may account for its divergence from the others.

One of the maps was read with an isodensitometer along the radial direction and the exposure verus radius is plotted in the same figure, with the anode plane as the abcissa and the ordinate representing positions toward the cathode. The distribution is certainly quite flat and falls off quickly at the edges. Possibly because the electric field in the diode is stronger in regions closer to the axis, the beam

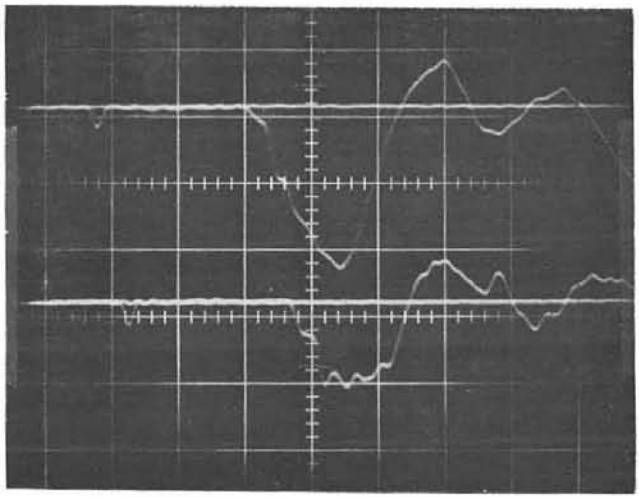

Current Sensitivity - 52 kA/cm
I_{peak} = 127 kA

Voltage Sensitivity - 1.18 MV/cm
V_{peak} = 1.53 MV

Sweep - 50 ns/cm

Figure 4.7 Tube Current and Voltage for Shot 3307

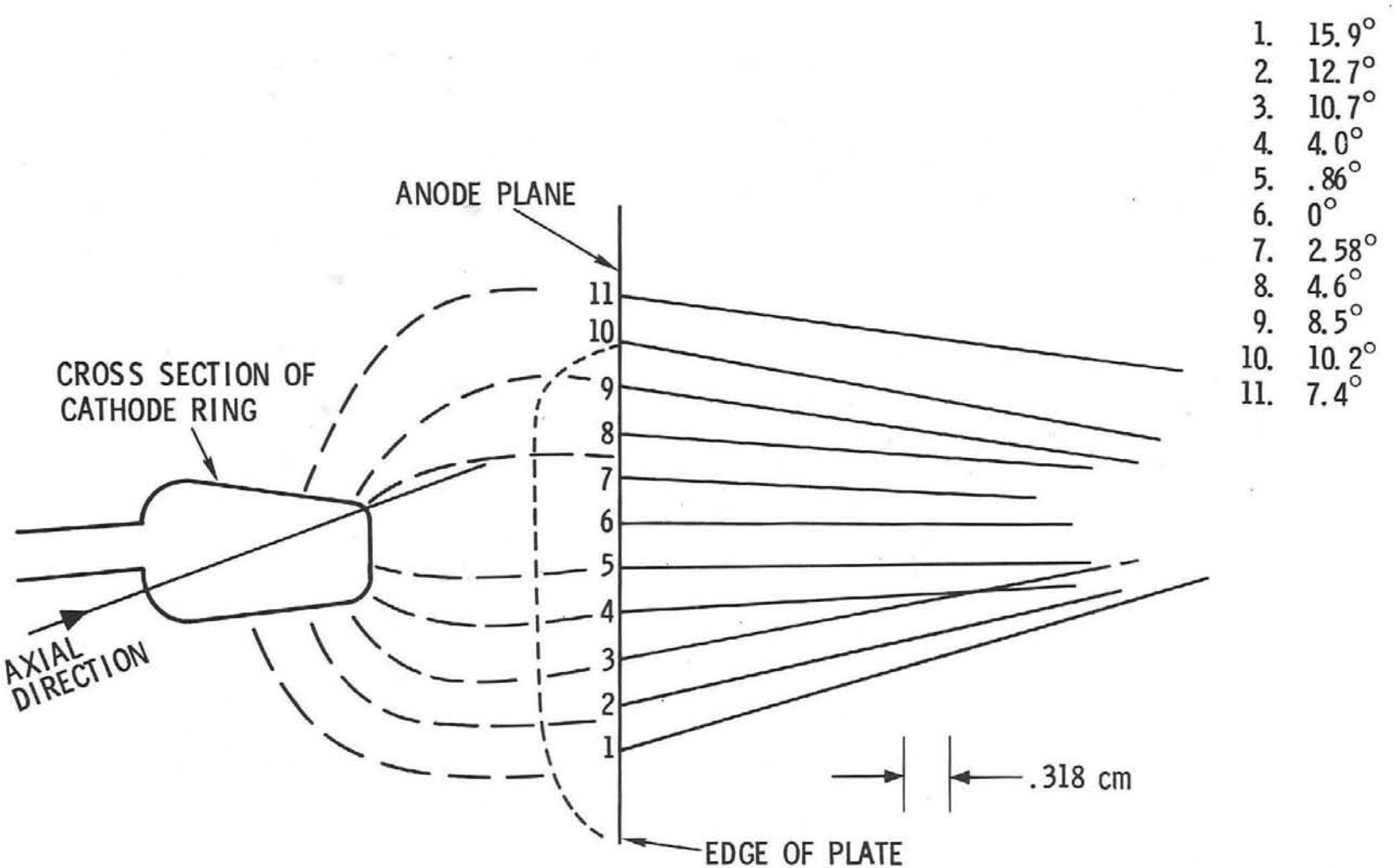

Figure 4.8 Analysis of the Mapping and Pinhole Results from Shot 3315

is seen to enter the drift channel on the average at a smaller radius than that opposite the cathode tip. The angles measured here were used in the choice of input conditions for the final computer calculations of the beam trajectories in the cones that were considered in Part I. At larger A-K gaps the beam would be more parallel, but the annulus would also be thicker.

The Search for a Narrower Beam and the Problems with Prepulse

A series of shots was now undertaken to find a way to make even a narrower beam despite the fact that we believe the currents from REBA were too low to keep the shank emitted electrons close to the emitting surface until they reached the cathode tip. A number of approaches could be taken. The radial thickness of the emitting tip could be reduced (as was done in shot 3315); a search could be made for a better emitting surface in hopes that it would be superior to the epoxy ring or the razor type (and therefore make shank emission much less than tip emission); or the A-K gap could be reduced. Some work was carried on in all of these areas.

The first effort involved an attempted to achieve a narrower beam by shortening the A-K gap. Immediately serious problems with reproducibility and uniformity were encountered that could not at first be correlated with anything. One shot would be quite uniform while another, under presumably identical conditions, would generate a beam which would suddenly come off one side of the cathode and short the diode. Fig. 4.9 shows the pinhole and mapping analysis of shot 3313 which is a typical, but mild, "bad" shot. These results provide even more information about bad shots than Fig. 4.6 did about good shots. For this particular shot the A-K gap was 0.955 cm, and the cathode emitting surface was a 1 cm wide strip of Aquadag that was sprayed on the brass ring.

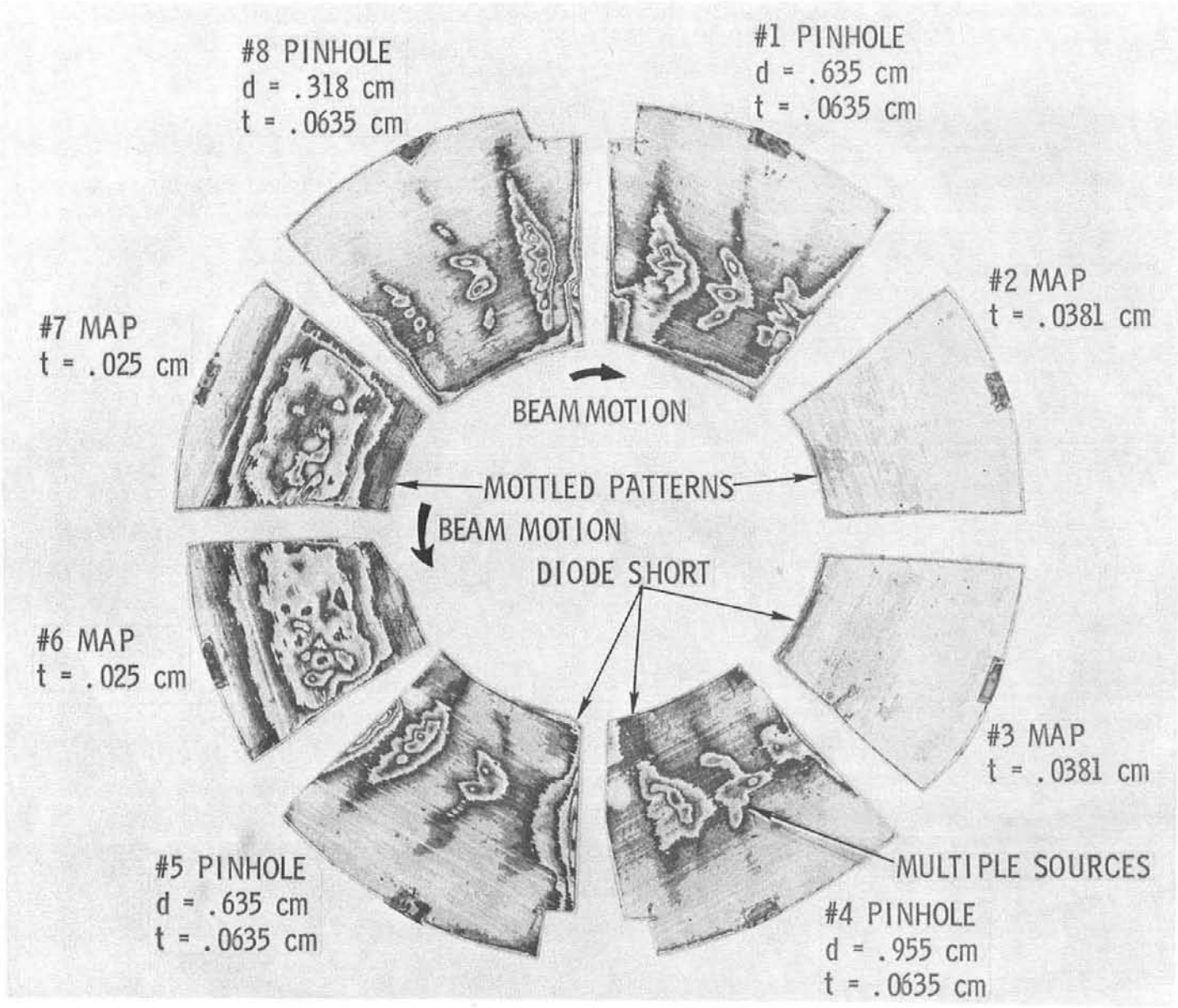

d = PINHOLE PLATE TO DOSIMETER SEPARATION
t = ATTENUATOR OR PINHOLE PLATE THICKNESS

Figure 4.9 Pinhole and Mapping of Shot 3313 at the Anode

#1. The spots not only pinch radially but also sideways very severely. The middle array of spots is particularly interesting because it appears that the spots are moving at a uniform speed and that the change in intensity along the path just reflects the change in beam current versus time. The left line of spots, however, has a dog leg which may imply a sudden increase of azimuthal angle. On the right there are multiple spots for each pinhole which must mean that the electrons are reaching the hole from multiple sources. The azimuthal angles reach greater than 60 degrees and there is no way that this beam could have been focused.

#2. The map exposure is much weaker than the corresponding ones of 3307 so the electrons had much less energy. Of course part of the reason must have been the higher angles of incidence on the attenuator. The structure is no longer uniform but is splotchy and mottled.

#3. This is much like the one above except that there is a more intense region near the inner beam boundary. There was a lot of physical damage here because, late in the pulse, the diode shorted to this spot. Note that many of the pinhole spots streak in this direction.

#4. Even more physical damage occurred at this plate and the beam shorted here also. One sees radial streaking, multiple sources, and sideways motion all superimposed. The electrons are going all directions.

#5. This is much like #1 except that the electrons are in even more of a hurry to pinch toward the shorted spot. (In all of these exposures the darkening at the edges is due to leakage around the Ti plate edges and the whitened spots are shadows from support structures).

#6. This map does show that the beam is narrower than it is at larger A-K gaps. However the pattern is more mottled. One can see how the two techniques (mapping and pinhole) complement each other here. This map does not present a very good conception of the angles of the electrons.

#7. This one is much the same as #6. It may be that multiple sources on small-scale instabilities are being seen here. The pinhole spot multiplicity seems to indicate that the multiple sources idea is the more likely explanation.

#8. The motion is less severe and it appears that less beam came from this position all during the pulse. The reduced sideways motion probably occurs because this octant is almost opposite the short and the electrons don't know quite which way to go.

The only correlation that was observed at first was that bad shots increased in frequency and became dominant as the A-K gap was reduced. Fianlly, using the voltage monitor, we began to measure the magnitude of the prepulse (which begins about 800 ns before the main voltage pulse while the Blumlein is charging). With the prepulse switches in place and a diode voltage monitor resistance of 550 Ω, the peak prepulse voltage varied between about 25 and 40 kV. The shots were then divided on the basis of uniformity and of current and voltage measurements into three catagories (good, neutral, and bad) and plotted in Fig. 4.10. Except for one deviant point, it is quite obvious that the correlation of prepulse to beam quality is very high and that we had been operating right around the threshold. The striking thing was that the division between good and bad shots was so narrow, i.e., only a 10 percent charge in prepulse level made the difference. It appears that for this configuration, once a prepulse of about 34 kV is reached (or an electric field of about 20 kV/cm), a few whiskers on the cathode will explode and launch a very bumpy plasma toward the anode. If one bump should reach the anode during the main pulse, the diode will short and all of the current will be drawn to that point. Even if a bump does not reach all the way to the anode, the field enhancement on its surface plus the closer effective A-K gap will cause more current to be emitted there and will lead to irregular emission. These measurements have had a profound effect on our understanding of the importance of prepulse control on beam quality at this laboratory. They led to

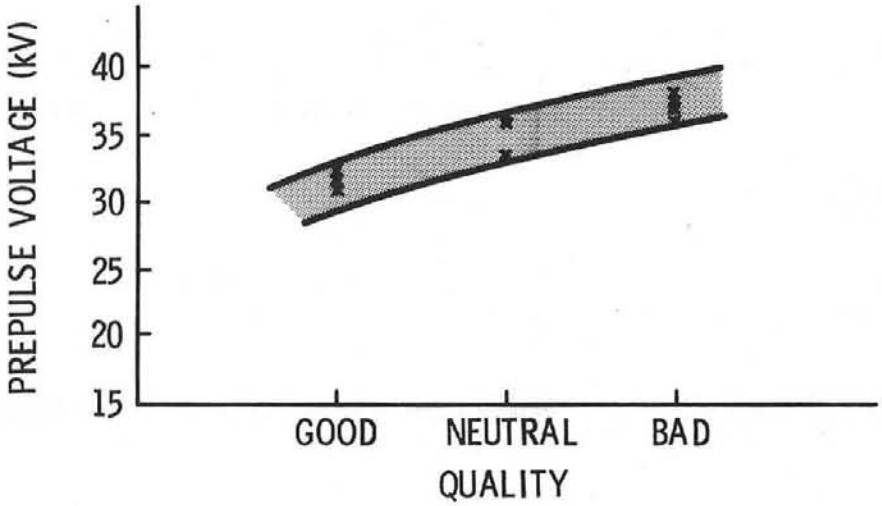

Figure 4.10 Correlation of Prepulse with Beam Quality

a realization of how the small diameter glass cathodes act as prepulse isolators so that high beam concentration at close A-K gaps could be achieved.[10] This was a picture which at the time was contrary to the model proposed by Bennett, et al.[11]

The most obvious way to reduce the prepulse would be to build a better prepulse switch, but that would have been too expensive and time-consuming then, so the resistance of the voltage monitor was reduced from 550 ohms to 40 ohms with the hope that the prepulse charge would drain off. With a diode impedance of around 6 ohms, 15 percent of the energy would be lost to that resistor. This is not a very satisfactory method, but it is simple. More reliable shots were obtained at 1.27 cm A-K gap and, when the beam was fired into a 4.5 cm wide cone channel, 1400 calories out of an input of about 1900 calories made it through a 7.5 cm diameter exit. This was a considerable improvement in performance over the first configuration and exhibited the highest transport efficiency achieved by any REBA diode up to that time, but it was still below the objective.

Mention was made earlier of the fact that the multiple spots are hard to see with the image quantizer readings so we have assembled for comparison three types of display of a pinhole and of a map sector. The three methods of illustration (photograph, image quantizer, and image differential mode) are shown in Fig. 4.11. The contour intervals are twice as close together here as they were in the other examples.

A few more attempts were made to get a narrow annular beam. The cathode ring was made even narrower with a primary emitting thickness of only 0.318 cm. Epoxy ring, Aquadag-coated ring, and single hoop razor blades were tried at distances between 0.635 and 1.27 cm with six inch long nylon prepulse isolators in the cathode shank. We were able to obtain fairly good shots at these very close spacings and the cone transport was fairly efficient, but there was very little energy in the beam. We believe that the extra prepulse system did work, but that the plasma launched by the main voltage pulse crossed the gap and

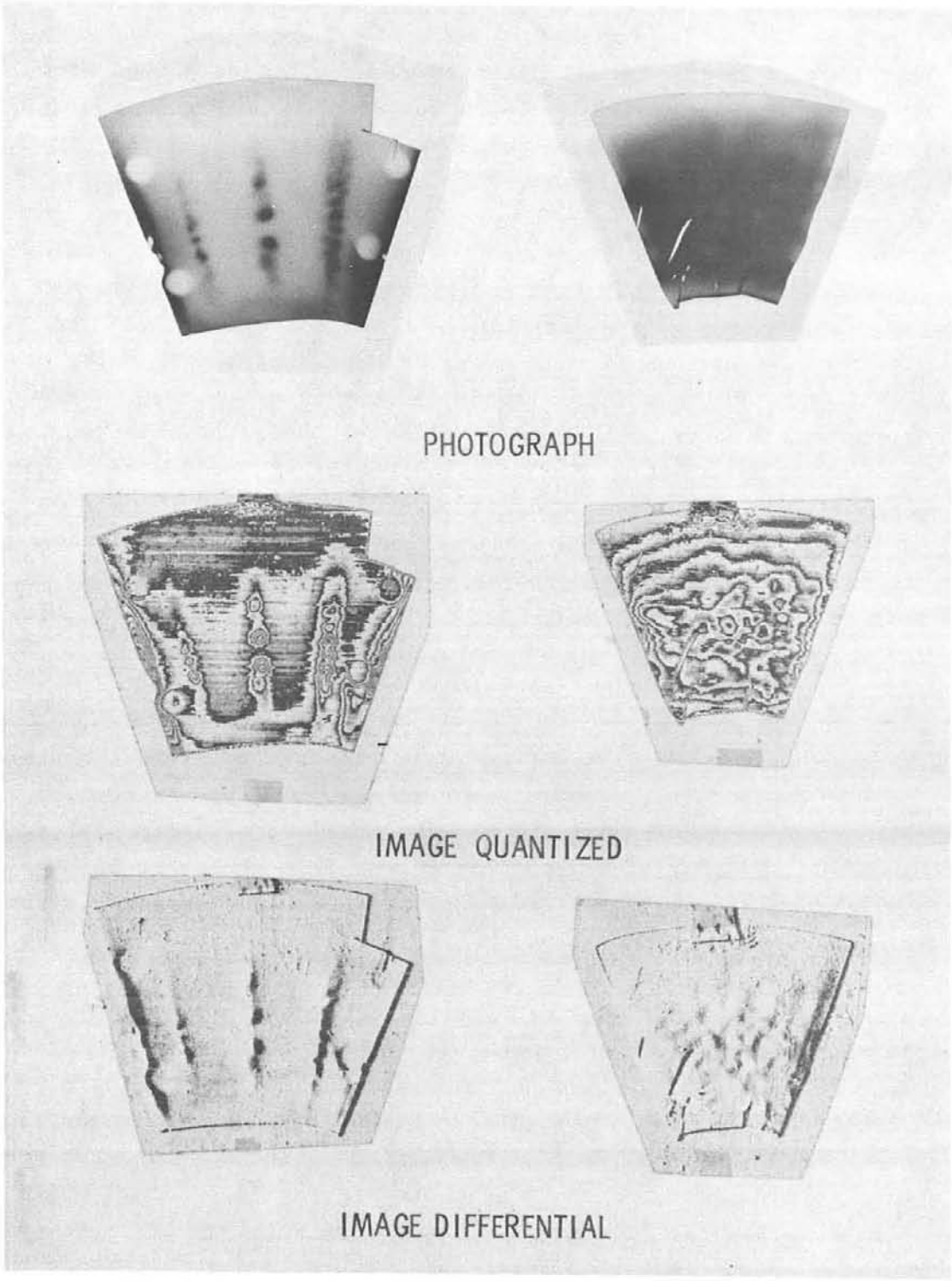

Figure 4.11 Comparison of Display Modes on Pinhole and Map Diagnostics

shorted the diode in a hurry. The short in these cases had an entirely different character than that caused by prepulse. The closing plasma was much more uniform, as if the main voltage exploded many whiskers instead of just a few. The short created little physical damage and there were no very dominant hot spots at the anode. Most of the energy was reflected back into the Blumlein.

A pinhole and mapping shot was taken at the anode with this narrow epoxy ring cathode with an A-K gap or 0.635 cm, and with the prepulse shank in place. The dosimeters are shown in Fig. 4.12. In a number of ways the beam has quite a different character from those generated with wider gaps.

#1. The exposure for this thin attenuator is much weaker than that obtained with larger gaps. Clearly the electron energy is much lower, probably in the neighborhood of 500 keV.

#2. There is sideways streaking here toward a hot spot that appears on this plate. However, the damage was negligible and only a minor fraction of the energy seems to have gone there. One real new feature is that, with only a couple of exceptions, the spots (even at maximum pinch) are more widely spaced than the pinholes. It is therefore possible to obtain both diverging and converging beams. The best cone transport is expected to take place with a parallel beam at the anode, and it is clear that this can be accomplished by trying different A-K gaps. Of course, that can only happen at one value of the current, presumably the peak.

#3. The mottled structure here illustrates the degree of non-uniformity of cathode emission. We believe that these patterns cannot represent the resistive tearing instability for the whole ring edge that generates the simple striations[12] produced by razors. The spatial frequency is too high for this ring thickness. However, another possibility may be that each sharp edge on this cathode emits like a razor and each separate sheet tears. When these many torn sheets overlap, they may give rise to this jumbled structure.

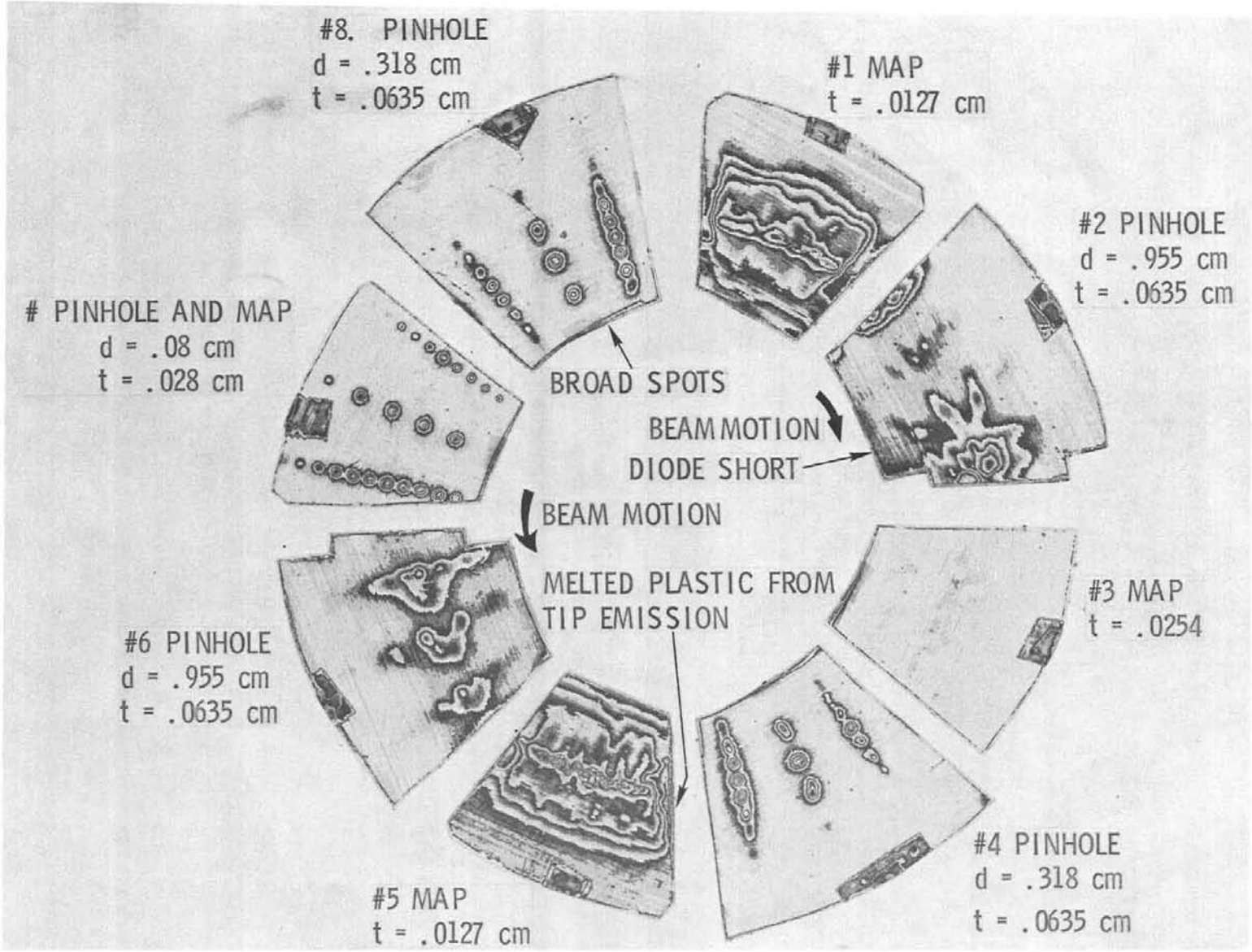

d = PINHOLE PLATE TO DOSIMETER SEPARATION
t = ATTENUATOR OR PINHOLE PLATE THICKNESS

Figure 4.12 Pinhole and Mapping of Shot 3792 at the Anode

#4. The beam here is slightly diverging and quite steady. The big change in all of these pinhole spots is th at the angular distribution of the electrons is so much broader through a hole than that with larger gaps. One explanation may be that the jumbled and torn sheets are still overlapping in space. With wider gaps the various components became separated so that electrons from only one source on the average strike on-hole. It was the results of this shot which caused us to go back and more accurately measure the spot positions on previous shots. It does turn out that there is a small average random variation in relative spot positions that leads to twice the average angle for the whole beam than that obtained from measurements of the angular distributions of individual spots alone. This total average angle was enough to account for the limits in focusing ability that we have seen. (See the next section of this chapter.)

#5. Both this map and #1 show two levels of intensity across the exposure. It appears that there is a real separation here between tip and shank emission. However, that may only be so just before the diode shorts because there is not nearly as much difference in the higher energy map #3. Also the total emission width including that from shank emission is the narrowest yet obtained.

#6. This recording is very much like #2 except in this case the beam stays straight and steady for sometime before the sideways motion begins.

#7. A shortage of undamaged map plates caused us to use an .028 cm pinhole plate for a map. The map exposure is very weak but similar to #3. The relative spot intensity also gives a good indication of the beam intensity profile.

#8. The same consistent broad distribution of the beam electrons is still evident.

Decreasing the A-K gap and reducing prepulse does allow us to generate a narrower and more parallel beam, but only at a great loss of energy delivered. For this 17 ohm machine this cathode was too large in area to maintain a high enough impedance when shank emission

contributes. Furthermore, the gap closure was so rapid that the diode impedance changed by an order of magnitude, from about 10 to 1 ohm, in a few tens of nanoseconds. If the shank emission could be eliminated, it might be possible to reduce the beam thickness and raise the impedance by making the emitting area thinner.

Transport and Compression in Cones

In the last section it was shown that, in the geometry available, fair uniformity was achieveable with small A-K gaps. However, the configuration was not useful because the impedance was too low for significant energy to be delivered to the diode. The gap was therefore moved back to 1.27 cm and a series of experiments were begun to test the properties of and the focusability of the best beam that had been achieved. The prepulse shaft was not needed with this gap. The main object was to see how much beam could be delivered through a hole about 6 cm^2 in area. The configuration for these tests is shown in Fig. 4.13. The channel thickness in this case was 1.6 cm. A Rogowski coil and a Faraday cup whose carbon stopping block was also a calorimeter were used to diagnose the properties of the existing beam. Also some appropriate pinhole measurements were made near the end of the cones.

The angular momentum present in the beam has been cited as the explanation for the limit on the focusability, but some direct comfirmation was needed. A pinhole package was constructed to fit in the channel near the end of the inner cone at the position P_1 shown in Fig. 4.13. If the electrons striking the plate possessed only r and z components of velocity, then the exposure pattern should consist only of a radial array of spots whose widths are the same as the hole diameters (.0159 cm). The actual pattern that was obtained is shown in Fig. 4.14. For this particular shot the drift channel pressure was 10 Torr and the A-k gap was 0.955 cm. Some observations follow.

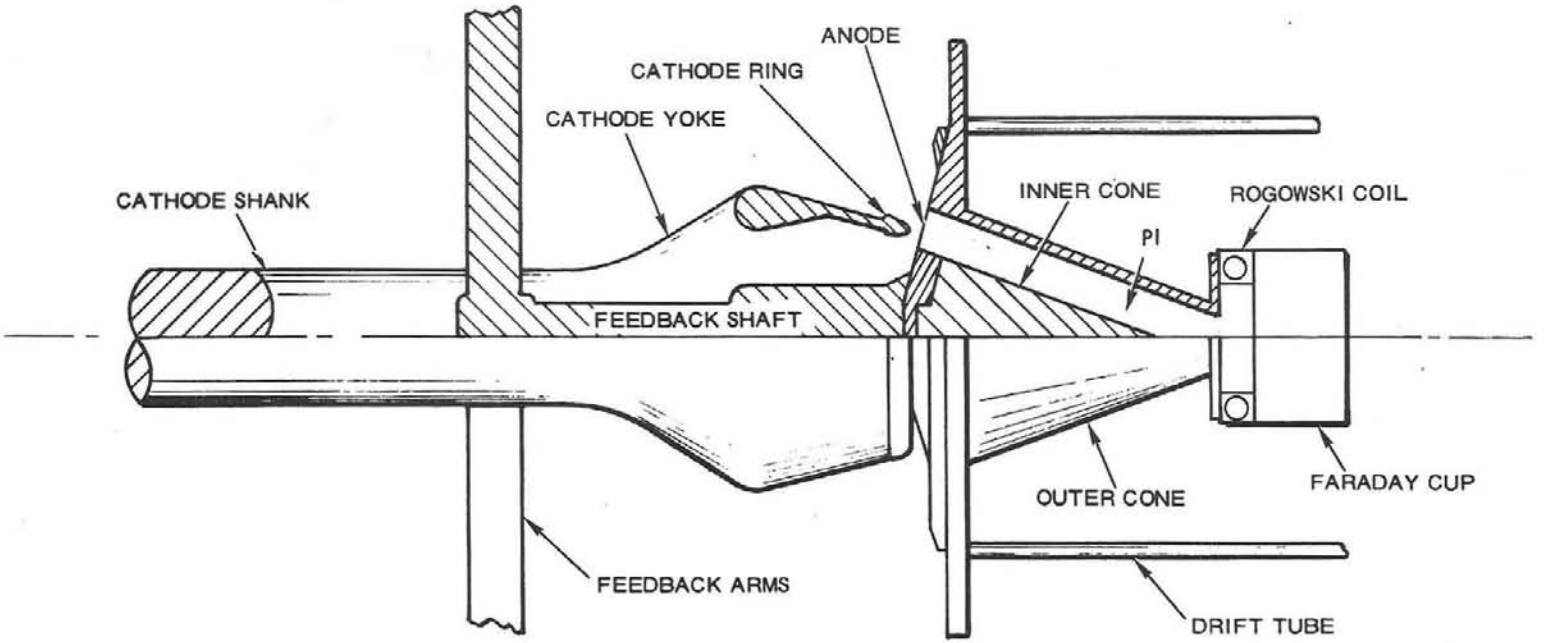

Figure 4.13 Diode and Diagnostic System Arrangement

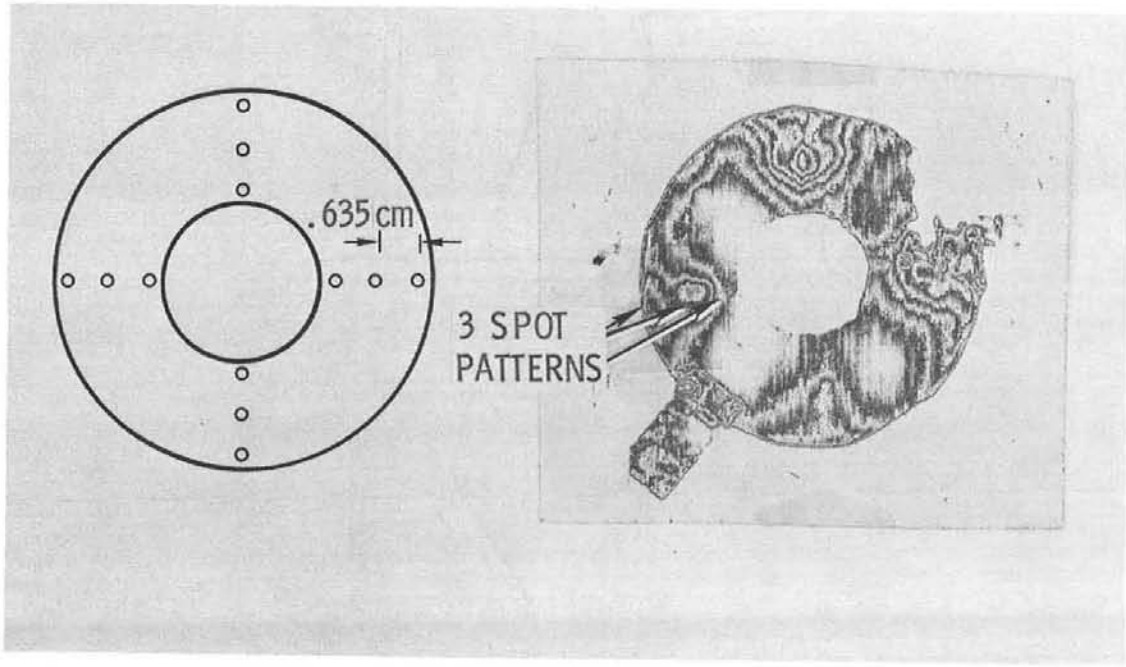

Figure 4.14 Pinhole Measurement Near the End of the Inner Cone

(1) The average beam direction is generally parallel to the channel but is drifting outward slightly.

(2) The overall azimuthal symmetry is fairly good because the average exposure on the four sets of spots is about the same within a factor of two.

(3) There is a spread of beam in the r,z plane just as one would expect if the usual sheet pinching became jumbled farther down the tube.

(4) Most of the beam is concentrated near the outer radii, and little exposure is seen from the inner holes.

(5) The spots are very broad azimuthally and reach angles beyond 45 degrees. It turns out that the 0.2 cm thick carbon pinhole plate cuts off angles larger than this so the actual angles are probably much higher.

(6) More careful examination reveals that the azimuthal angles tend to be larger at the larger radii, as one would expect when the electrons become sorted in radius according to their angular momentum near the end of the cone.

(7) There is some fragmentation of the beam as evidenced by the tendency for multiple spots from a hole. (This multiple spotting can only be seen by observation at the dosimeter itself.)

Another pinhole measurement was made at the end of the outer cone. Examination leads to the same conclusion. The beam is azimuthally hot and cannot be compressed without serious loss of beam. However, the maximum intensity occurred on the axis so the colder electrons that remained in the beam were being properly focused.

A survey of beam transport in the cones versus pressure covered the region from 0.1 to 20.0 Torr. Again the A-k gap was 1.27 cm. At this gap the beam thickness is much wider than the opening to the cones so that only about 1100 of the 1700 calories generated by the diode entered the channel. The data from one of the shots in the survey is discussed below.

Figures 4.15, 4.16, 4.17, and 4.18 are the oscillograms of the electrical diagnostics for shot 3800 at 1 Torr pressure. The monitor for the total current, I_T, was mounted in the diode just behind the feedback arms. The tube voltage monitor was connected to ground from the base of the cathode shank. The voltage trace has not been corrected for tube inductance.

Just behind the anode plane but in front of the feedback bars was a Rogowski coil for monitoring the current in the outer circuit before the axial current was included. The top oscillogram in Figure 4.16 indicates that indeed about half of the total current did flow in the outer wall of the diode. The peak value of the prepulse voltage shown in the lower trace is 20 kV, well below the usual threshold of about 34 kV. The shot was a good one.

Beyond the end of the cone the Rogowski coil and the Faraday cup were mounted as shown in Fig. 4.13. The trace in Fig. 4.17 from the Rogowski coil shows the typical net current curve for a beam which becomes highly current neutralized. After the initial steep rise, the gas breaks down suddenly as the plasma return current begins to flow. The net current reached a peak of 8 kA and then decayed slowly, long after the primary current was gone, as the decreasing B_φ field continued to drive plasma current (now in the forward direction). The Faraday cup whose current is shown in Figure 4.18 had a Kapton film window on its face which was intended to block the plasma current so that the cup would measure only the primary beam. It recorded a peak current of about five times that of the Rogowski coil and showed no long tail. Other Faraday cupcurrents show a variety of forms that provide a measure of focusing efficiency versus time at each pressure. An example of this will be shown later.

The calorimeter mounted in the Faraday cup recorded a total energy deposition of 520 calories which is about half of the energy injected into the cone channel.

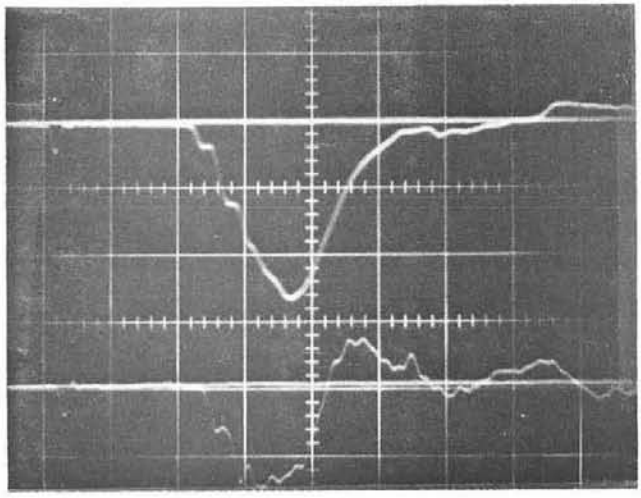

Tube Current - 52 kA/cm
I_{peak} = 159 kA

Tube Voltage - 1.18 MV/cm
V_{max} = 1.83 MV

Sweep - 50 ns/cm

Figure 4.15 Tube Current and Voltage for Shot 3800

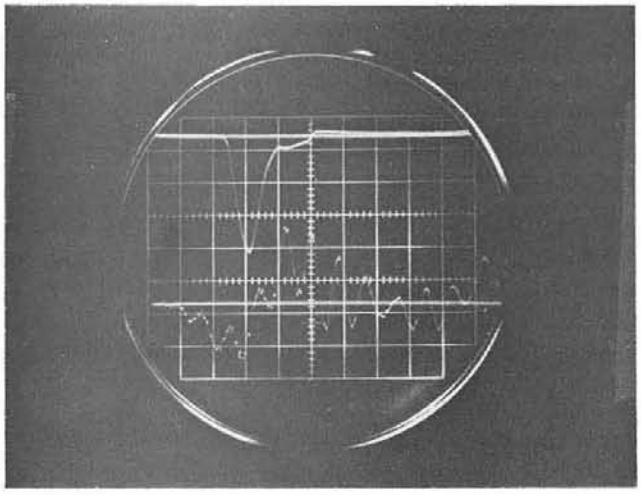

Outer Wall Current - 24.8 kA/cm
I_{peak} = 87 kA

Prepulse Voltage - 12 kV/cm
V_{max} = 20 kV

Sweep - 50 ns/cm

Figure 4.16 Outer Wall Current and Prepulse Voltage for Shot 3800

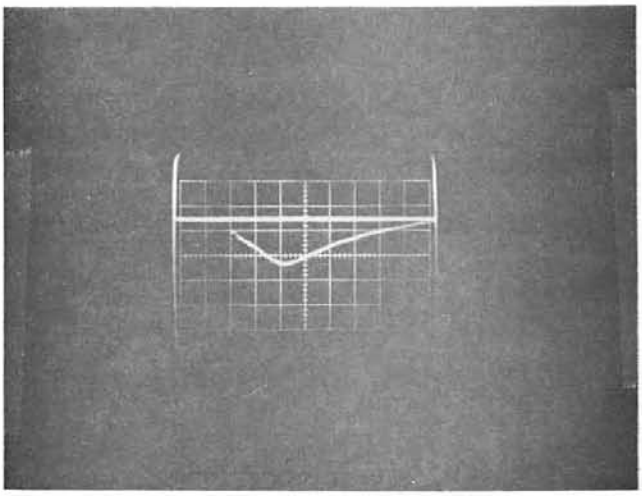

Rogowski Coil Current - 4.5 kA/cm
I_{peak} = 8 kA

Sweep - 50 ns/cm

Figure 4.17 Net Cone Exit Current

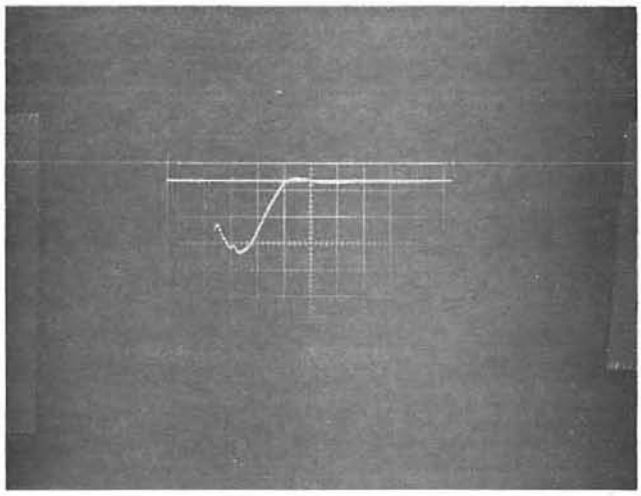

Faraday Cup Current - 14.1 kA/cm
I_{peak} = 38.2 kA

Sweep - 50 ns/cm

Figure 4.18 Primary Cone Exit Current

The reader may recall that in the Triax design concept the transport efficiency is expected to have only weak dependence on beam current or electron energy. One would expect therefore that the cone transport and compression efficiency would have only a weak dependence on the pressure. Figure 4.19 shows that this is indeed the case. Each of the points on the graph, that are far below the curve, has been verified to be either the result of the occasional lower machine output or of nonuniform emission. It is fairly obvious that tuning the system with pressure will not yield much improvement in efficiency.

The Effect of Radial Vanes in the Channel

If the angular momentum is really the limiting factor in the focusability of the beam, then it is worth the effort to attempt to control or reduce it. If the angular momentum is really an initial condition, then non-radial forces must be introduced. One possible way to do this would be to apply an external conical B_z field which would guide the beam toward the focus. This route has been superficially explored and it appears that the best approach would be to preionize the drift channel gas to freeze the magnetic field lines and suppress the instability growth. However, at the present time there are no plans to try this approach.

A potentially easier method was to introduce radial vanes into the channel. The annulus was divided into eight equal sectors. At four boundaries, 9 cm long steel vanes were placed (in the r,z plane) and, at the other four alternating boundaries, 3.5 cm long vanes were positioned. The intention was to determine whether a division of the annular beam into multiple guided beams that could afterwards be superimposed would lead to better success than that achievable with the basic Triaxial system. Only one comparison was made (with and without vanes) and that was at a pressure of 5 Torr, with an epoxy ring cathode and an A-K gap of 1.27 cm. The oscillograms of the Faraday cup current of the two shots are compared in Fig. 4.20. It is

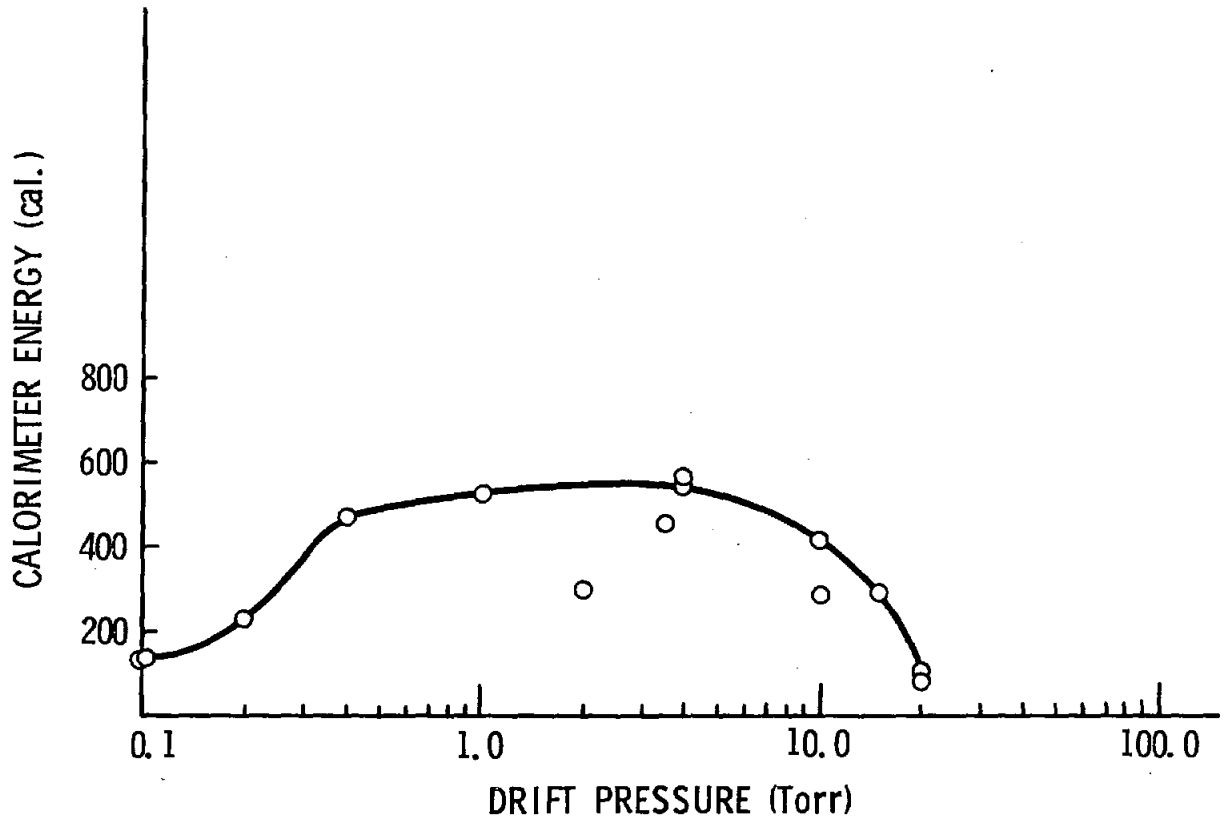

Figure 4.19 Energy Delivered to the Calorimeter vs. Drift Pressure

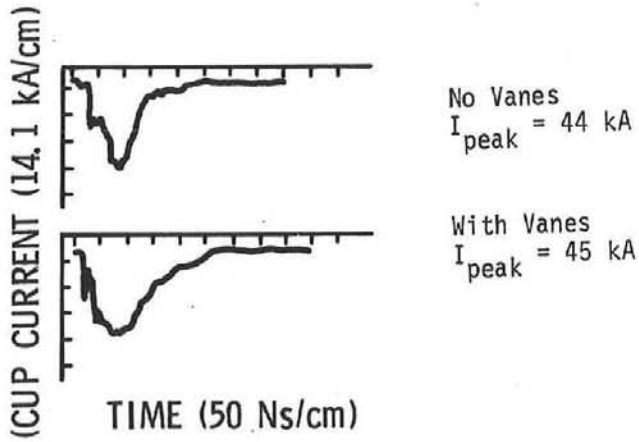

Figure 4.20 Comparison of Triax System Currents with and without Channel Vanes

quite clear that, although the current reaches the same peak value in both configurations, the beam is focused properly when the vanes are in place only over a narrow span of time. The calorimeter on the no-vane shot recorded 575 calories and with the vanes it recorded 260 calories. The vanes themselves were severely spalled in alternate spots down the channel as though the divided beams were bouncing and fishtailing while losing energy to the vanes.

The investigation was not pursued any further, but the result is similar to that of some other (unpublished) experiments. It seems that as one attempts to guide a beam more strongly with more conducting walls, such as with vanes or multiple cone channels, the guidance can be done rather efficiently, but only over much more restricted parameter ranges. Two examples are the following. The transport efficiency versus pressure curve becomes very narrow and in addition good focusing occurs only when the electrons enter the channel in exactly the right directions.

Discussion and Conclusions about the REBA Triax System

The following is a summary of the major results of the second set of experiments with the REBA Triax.

(1) The modification of the cathode yoke to reduce azimuthal ring currents was a very successful change. The emerging beam was uniform in its gross structure and was directed down the channel.

(2) A narrow beam is difficult to obtain because of three factors. First, the emission does not just come from the tip; it also comes from the shank. Second, the REBA current is not high enough to create strong enough magnetic fields to confine the electrons close to the shank surface. Third, prepulse and diode plasma closure prevent the use of very close A-K gaps. (Also, at close A-K gaps, the emitting area even with narrow rings is too large to give proper diode impedance, ~17 ohms.)

(3) The pinhole and mapping techniques developed for this system yielded superior information about beam quality. They made it possible to tell the difference between "good" and "bad" shots and therefore provided the association with prepulse level. From these diagnostics, the input conditions for the computer calculations of Part I were obtained.

(4) The small-scale mottled and splotchy nonuniformity in the diode emission was found to be enough to account for all of the limit of the focusability of the beam; it has not been necessary to invoke arguments about the growth of instabilities in the drift channel, although we believe they are sometimes seen on bad shots.

(5) The electrons coming from the diode seem to come from many almost-independene sources on a spatial scale of 0.3 cm for razor, epoxy ring, and Aquadag-coated cathodes. Where the beamlets from sources overlap, multiple pinhole spots appear. Some means of reducing the scale of nonuniformity must be found if the system is to be very useful.

(6) The prepulse level can be reduced by lowering the resistance of the voltage monitor and by placing a dielectric switch in the cathode shank.

(7) A beam, whose electrons strike normal to the anode surface, is obtainable but in this configuration it has not been achieved with good diode impedance match.

(8) Under the best conditions the beam entering the cone has been compressed by a factor of ten in area with 50 percent efficiency.

(9) The efficiency has only a weak dependence on drift channel pressure as would be predicted by theory.

(10) Guiding vanes introduced into the channel do not improve the focusability except possibly for a very restricted set of parameters such as pressure, current (a strong function of time), electron spatial and angular distribution, electron energy, etc.

One way to improve the REBA Triax would be to redesign the diode in the following manner. A sketch of a diode with a small cathode ring and a convergence angle of 30 degrees is shown in Fig. 4.21. The average angular momentum depends on r and, if one assumes that the average velocity of the electrons remains the same, the minimum radius should go down by a factor of 0.6. The same yoke could be used as in the previous configuration and the impedance would be higher so that the smaller A-K gaps could be used without nearly as much impedance mismatch energy loss. The channel length is also only about half as long as before and any instabilities in the drifting beam would have less time to grow.

The central problem that remains is the azimuthal symmetry of the beam as it is generated in the diode. Since the beam appears to emerge from a multitude of small almost independent sources, the uniformity should be improved by multiplying those sources. However, our attempts to introduce more emitters by using Aquadag on brass cathodes did not lead to significant improvement. The reason may be that beyond a certain point this high-impedance, 17-ohm machine just cannot supply enough current to light up all the emitting whiskers. Futhermore, the secondary problem of beam thickness can be better handled by a higher-current, lower-impedance machine. For the above reasons and also because the Hydra machine (for which the Triax system was conceived) was coming on line, the work was shifted to the new machine and a new Triax diode.

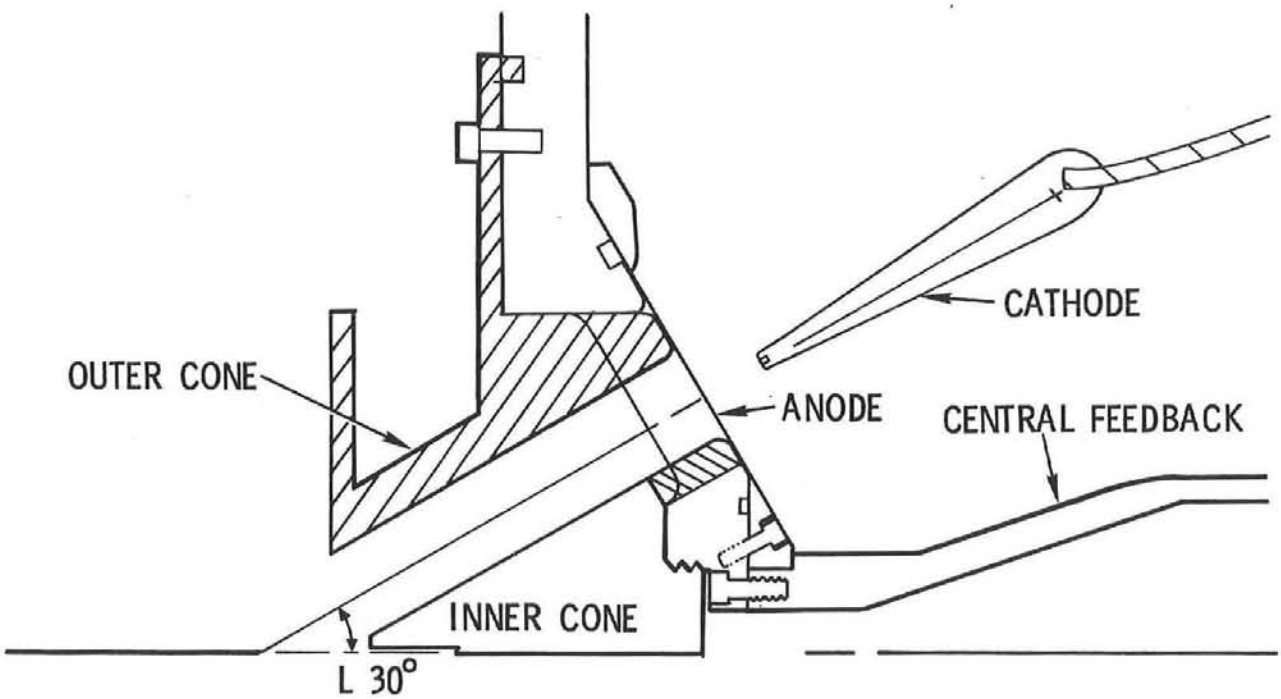

Figure 4.21 Proposed Third Version of the REBA Triax

CHAPTER V - THE HYDRA TRIAXIAL DIODE

The Hydra Accelerator and the Design of the Diode

The Hydra Accelerator, like REBA, is composed of a Marx generator, a pulse forming line, and an output diode. However, in this case there are two pulse forming lines and diodes which are of much lower impedance. The nominal design parameters were a peak voltage of 1 MeV and peak current of 500 kA per line for about 70 ns. A sketch of the facility is shown in Fig. 5.1. Its features have been detailed in a previous report.[13] One of the most important new features of this machine, which was expected to be very important for the operation of the Triaxial diode, was the prepulse switch that was mounted near the diode end of the pulse forming line. This switch is composed of six gas-filled spark gaps that were expected to reduce any prepulse voltage to less than 500 volts. With this level of prepulse, plasma should not be generated in the diode until the main voltage pulse arrived. If the (until recently accepted) plasma closure velocity of about 2 cm/μsec is used to calculate the diode shorting time for an A-K gap of 0.635 cm, one finds that the diode should stay open for 300 ns. This seemed at the time to be an adequate margin of safety, so the diode was designed for this gap.

The Child-Langmuir law for space charge limited flow can then be used to calculate the cathode area which will give an impedance of 2 ohms. That law in mks units for plane equal area anode and cathode surfaces, A, is

$$I = 2.33 \times 10^{-6} \frac{A}{d^2} V^{3/2} . \qquad (5.1)$$

I is the diode current, d is the A-K gap, and V is the tube voltage. Putting in $V = 10^6$ volts, I = 500 kA, and d = 0.635 cm, the area is found to be 86 cm^2. Shank emission is very difficult to estimate but nevertheless a cathode with about 60 cm^2 emitting area was designed with the assumption that the shank would supply an extra 25 cm^2 of

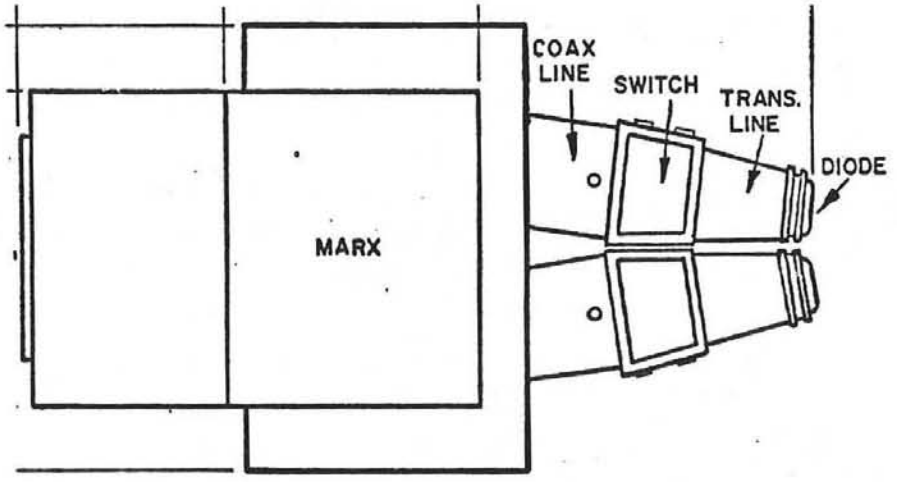

Figure 5.1 The Hydra Accelerator

emitting area. The ring radius was made to be about 10 cm in diameter so that it would both fit the existing diode chamber size and also generate a beam with less initial angular momentum than the REBA diode did. However something was sacrificed by choosing this small diameter ring. Even though the pinching is reduced when current is fed back along the axis, an analysis similar to the calculation of the Triaxial Alfvén limit carried out in Part I, page 27, revealed that the beam from this diode would be mildly sheet-pinching at the anode. This dilemma in the choice of ring size actually exhibits what is one of the primary advantages of the Triaxial geometry over the flat cathode design. An extra parameter, the sheet thickness, is available for controlling the generation of the beam. It is, therefore, possible in principle to vary the ring diameter, shape, and thickness so that a parallel beam can be obtained at the anode for almost any chosen current. However, again the angular momentum that is present initially in the beam sets a practical limit on the cathode diameter. It was felt that in the Hydra case the mild pinch would be easier to handle than the angular momentum produced by a large ring.

The machine assembly drawing for the Hydra diode is shown in Fig. 5.2 in slightly larger than 1/4 scale. From the cathode base plate (23) five support posts (24) passed through five tubes (20). The cathode ring was mounted onto the posts with a slip fit so that no bolt heads or sharp edges appeared anywhere on the cathode system. The five tubes replaced the feedback arms of the REBA diode and, because the spacings between conductors are so much closer in this diode, these five tubes were able to support the entire central feedback structure. The principal advantage of this was that the supporting ribs at the anode window could be mounted from the outside of the diode simply by stretching the anode window with the disk (Part II in the drawing) until it sealed against the O-ring. The bolts were then pushed through the window to hold it in place.

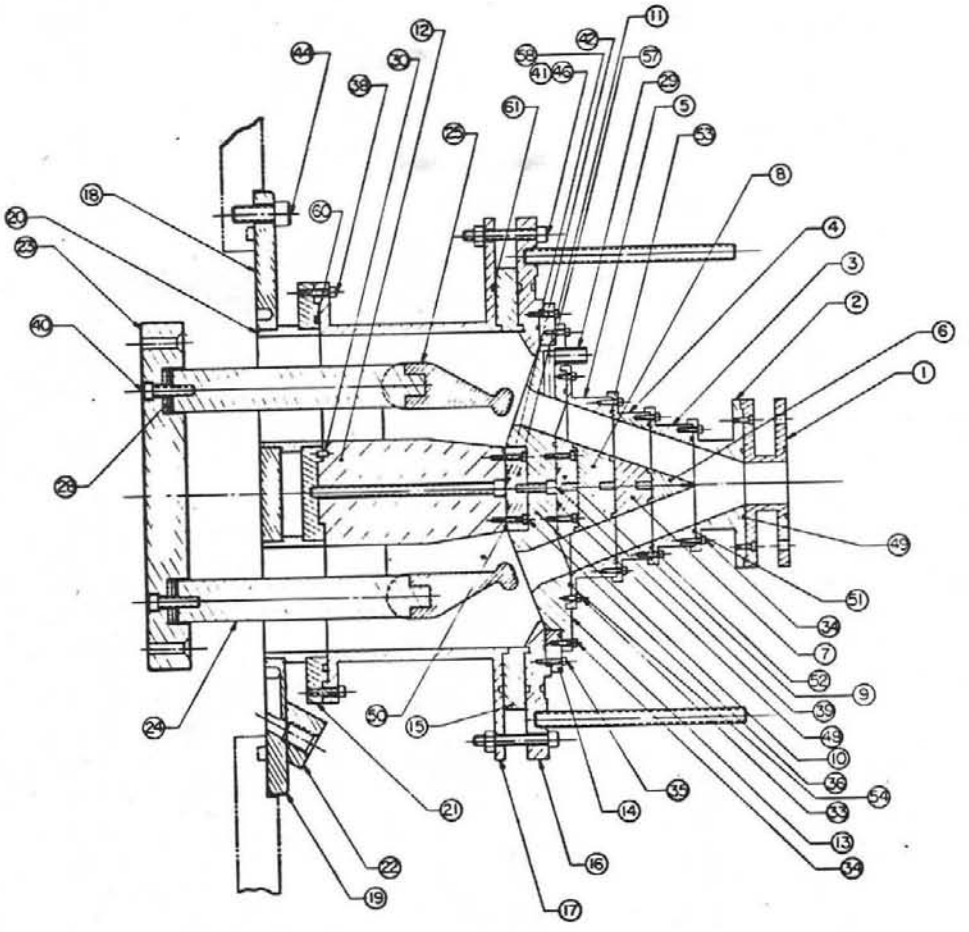

					62
3		O-RING, VITON, 9.500 I.D. × 1/8 DIA			61
1		O-RING, VITON, 8.250 I.D. × 1/8 DIA			60
					59
1		O-RING, VITON, 1/16 DIA, BULK STK			58
1		O-RING, VITON, 1/16 DIA, BULK STK			57
					56
					55
1		O-RING, VITON, 4.500 I.D. × 1/16 DIA			54
1		O-RING, VITON, 3.500 I.D. × 1/16 DIA			53
1		O-RING, VITON, 2.875 I.D. × 1/16 DIA			52
2		O-RING, VITON, 2.000 I.D. × 1/16 DIA			51
1		O-RING, VITON, 1.750 I.D. × 1/16 DIA			50
1		O-RING, VITON, 1.500 I.D. × 1/16 DIA			49
1		O-RING, VITON, .750 I.D. × 1/16 DIA			48
					47
8		NUT, PLAIN, HEX., 1/4-20UNC			46
					45
12	MS16995-81	SCREW, SOC. HD., 3/8-16UNC × 1.000 LG			44
					43
1		SCREW, SOC. HD., 1/4-20UNC × 4.375 LG			42
8	MS16995-55	SCREW, SOC. HD., 1/4-20UNC × .750 LG			41
5	MS16995-52	SCREW, SOC. HD., 1/4-20UNC × 1.000 LG			40
1	MS16995-12	SCREW, SOC. HD., 10-32UNF × .750 LG			39
8	MS16995-28	SCREW, SOC. HD., 8-32UNC × .750 LG			38
					37
4	MS16995-20	SCREW, SOC. HD., 4-40UNC × .750 LG			36
12	MS16995-9	SCREW, SOC. HD., 4-40UNC × .625 LG			35
24	MS16995-18	SCREW, SOC. HD., 4-40UNC × .500 LG			34
4		SCREW, SOC. HD., 4-40UNC × .312 LG			33
					32
					31
1	MS16562-425	PIN, STRAIGHT, 1/8 DIA × .375 LG			30
1		TUBE, STAINLESS STEEL, 3.200 O.D. × .028 WALL			29
AR		SPACER			28
					27
					26
1		PLATE, BRASS, 1/2 H			25
5		ROUND, BRASS, 1/2 H			24
1		PLATE, STAINLESS STEEL, TYPE 304			23
1		ROUND, STAINLESS STEEL, TYPE 303			22
1		PLATE, STAINLESS STEEL, TYPE 304			21
5		TUBE, STAINLESS STEEL, TYPE 304, 3.000 OD			20
1		PLATE, STAINLESS STEEL, TYPE 304			19
1		WELDMENT			18
1		PLATE, STAINLESS STEEL, TYPE 304			17
1		PLATE, STAINLESS STEEL, TYPE 304			16
1		PLATE, STAINLESS STEEL, TYPE 304			15
1		PLATE, STAINLESS STEEL, TYPE 304			14
1		PLATE, STAINLESS STEEL, TYPE 304			13
1		ROUND, STAINLESS STEEL, TYPE 303			12
1		ROUND, STAINLESS STEEL, TYPE 303			11
1		PLATE, STAINLESS STEEL, TYPE 304			10
1		ROUND, STAINLESS STEEL, TYPE 303			9
1		PLATE, STAINLESS STEEL, TYPE 304			8
1		PLATE, STAINLESS STEEL, TYPE 304			7
1		ROUND, STAINLESS STEEL, TYPE 303			6
1		PLATE, STAINLESS STEEL, TYPE 304			5
1		PLATE, STAINLESS STEEL, TYPE 304			4
1		PLATE, STAINLESS STEEL, TYPE 304			3
1		PLATE, STAINLESS STEEL, TYPE 304			2
1		PLATE, STAINLESS STEEL, TYPE 304			1
NA	99-211-9	WELDING, STEEL			
NA	9900000-09	GENERAL REQUIREMENTS			

Figure 5.2 Machine Assembly Drawing of the Hydra Diode

The much closer spacings between the cathode and the ground planes were made possible because of the lower voltage and higher current of this machine. The magnetic field around each post and the ring provided magnetic insulation. This insulation was not effective at a few places such as along the axis between the cathode base plate and the base of the feedback shaft. This is the reason for the large separation there.

Beyond the anode, provision was made for the mounting of a second window so that for the first 2.5 cm of travel a different pressure could be maintained than in the rest of the drift channel. The main reason for this was the intention to control the diode sheet pinch as illustrated in Fig. 5.3. If the beam is pinching when it enters the drift region, it will just drift outward to the channel walls unless there is enough B field (net current) to turn them back. The first chamber was, therefore, designed to be kept at a low pressure so that the electrons would arrive at the second window with trajectories approximately parallel to the channel. Then, if the next drift region were set at a current neutralizing pressure, the beam would drift on freely toward the focus. Only the experiments could really prove the usefulness of this approach.

For the rest of the drift channel, the cones were sectioned so that the beam could be easily diagnosed at intervals. For active diagnostics, one Rogowski coil for the tube current was mounted at the base of the five tubes and another for the outer wall current was mounted at the anode.[15] Their difference yielded the central feedback current. Behind the cathode base plate were resistive and capacitive voltage monitors. At the end of the cones a Rogowski coil, Faraday cups, calorimeters, and pinhole and mapping packages could be mounted.

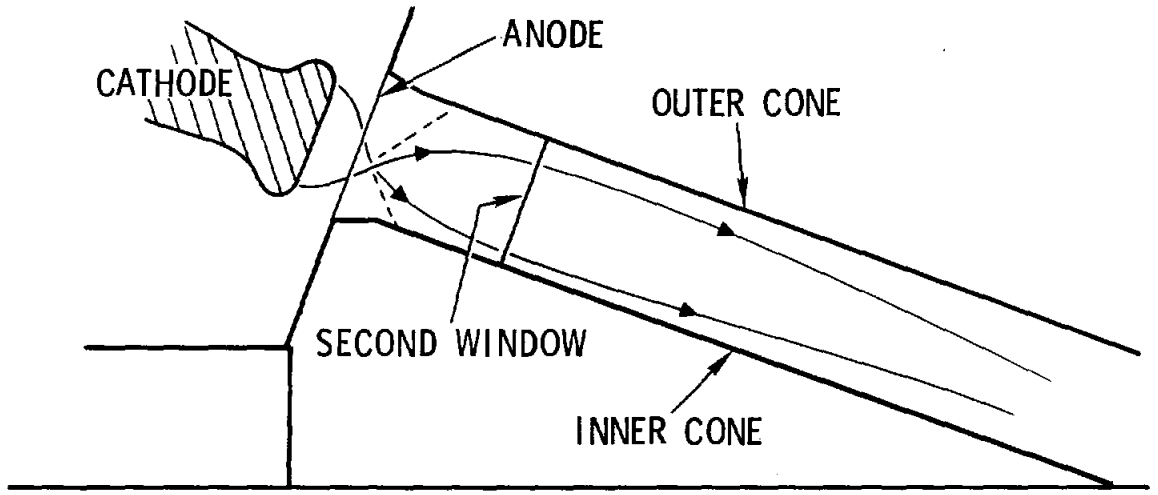

Figure 5.3 Trajectory Control with Chamber Pressure

The Experiments with the Hydra Diode

The prepulse switch on Hydra was expected to prevent diode plasma formation during the charging of the transmission line and for this reason the early shots were made at the small A-K gaps with epoxy ring cathodes.

At the 0.5 cm gap the emission was grossly very uniform and clearly entered the channel without loss to the entrance. It appeared to propagate efficiently at 1 Torr down to the last cone section where at a diameter of 4 cm it began to spall the tube walls. However, only 50 calories arrived at the Faraday cup (whose collector was also a calorimeter) and, even though the peak voltage was 882 kV and the peak current was 300 kA, the shortness of their traces revealed that the diode shorted in about 30 ns. It is quite clear that the diode plasma was closing the gap at a rate of about 15 cm/μ sec rather than 2 cm/μ sec (unless a plasma is launched during prepulse at only 500 volts which has not been shown). The same configuration was investigated with the 0.2 cm thick carbon pinhold plate shown in Fig. 5.4. The dosimeter was placed 0.635 cm behind the plate. The spot patterns in Fig. 5.5 and 5.6 indicate a diffused and mildly erratic beam that is fairly uniform around the annulus. It had sharp boundaries because only the holes near the central radius produced spots. This means that the magnetic insulation was effective. The intense darkening of the dosimeter with so little beam energy implies low electron energy.

The very broad distribution is still the mystery here, but when the diode plasma which is presumed to be bumpy is about to close it does seem likely that the electrons that are accelerated across the narrow and wavy gap will be sprayed over a wider range of angles.

The only choice at this point was to work at larger A-K gaps again. However, even though the pinhole spot size decreased as the gap was increased to 1.00 cm, 1.27 cm and 1.59 cm, the beam quality

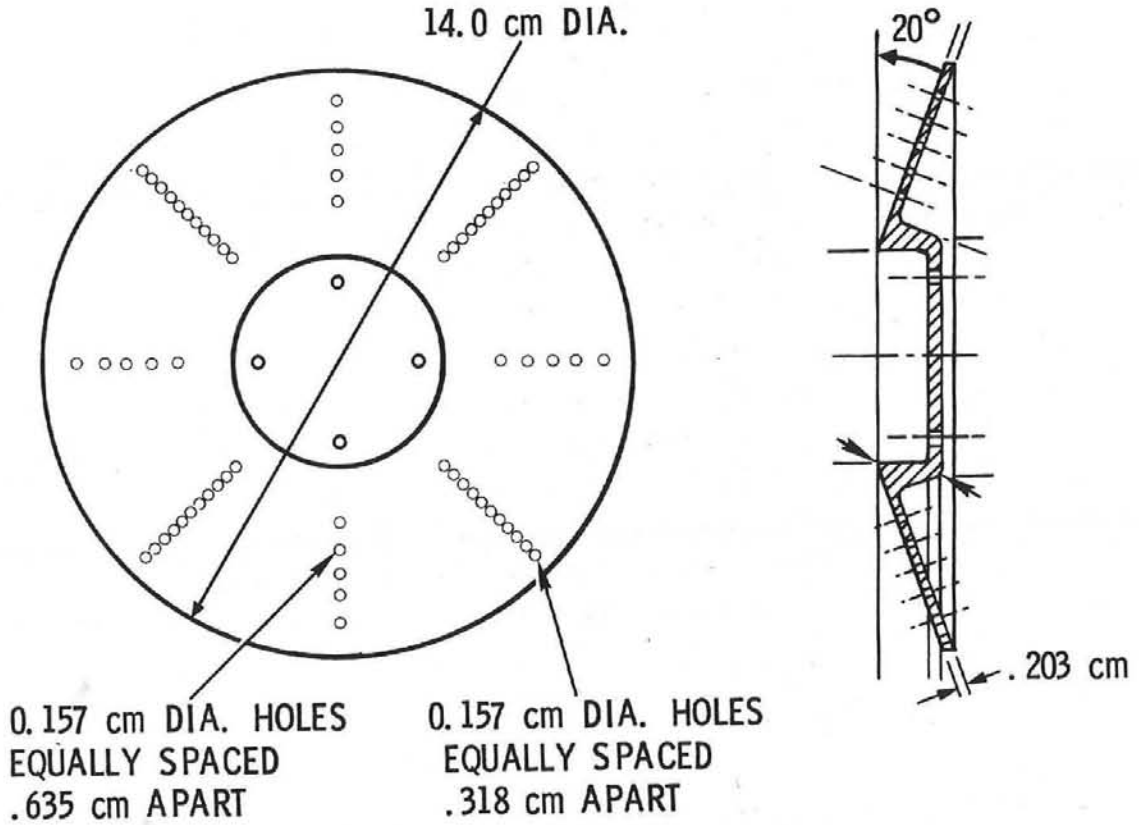

Figure 5.4 The Hydra Carbon Pinhole Plate

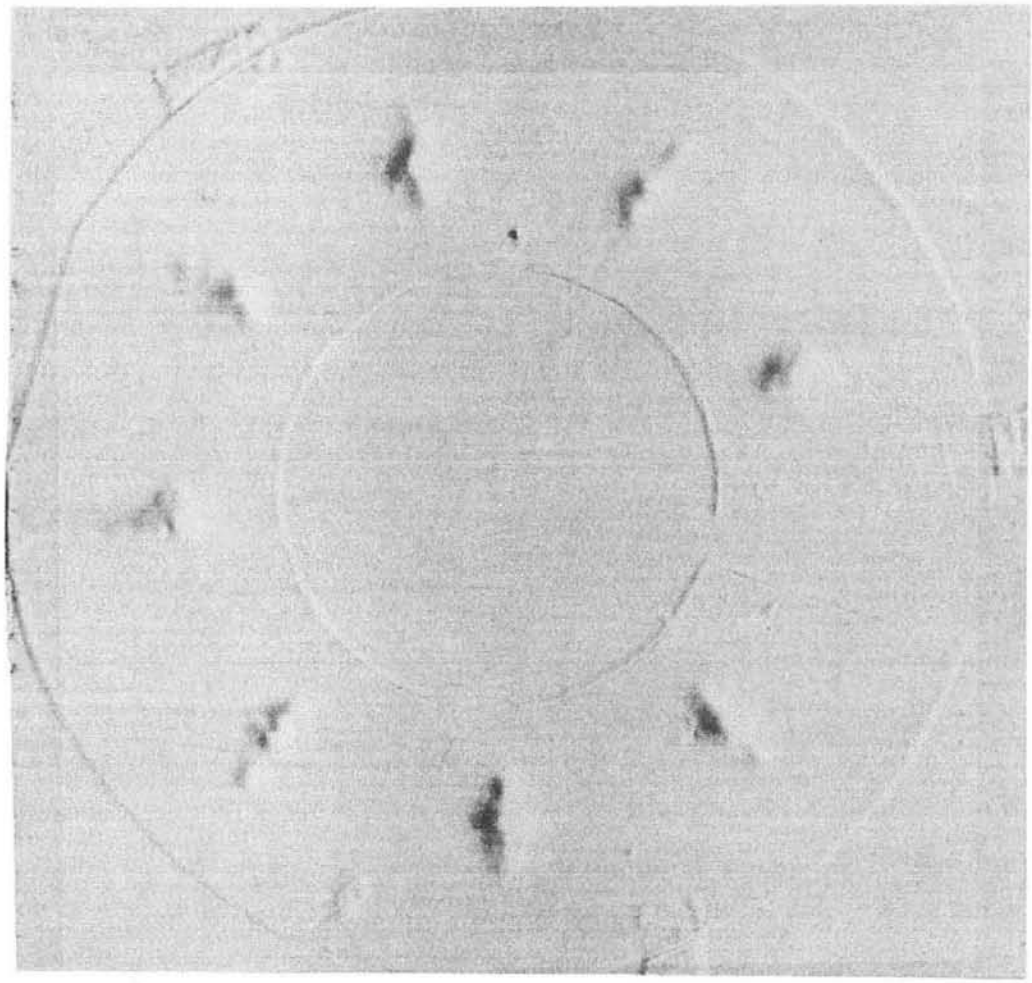

Figure 5.5 Pinhole Exposure of Shot 155 at
A-K Gap = 0.5 cm - Differential Mode

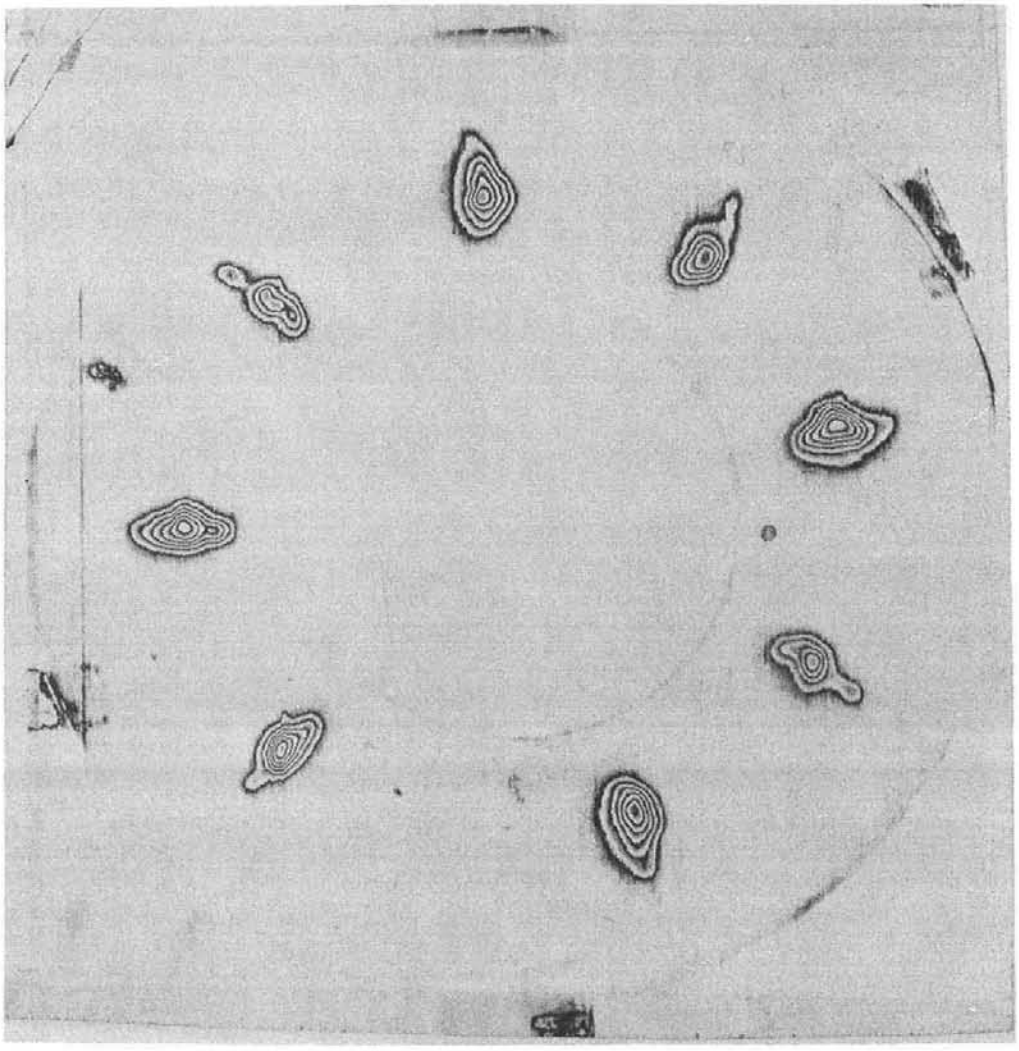

Figure 5.6 Pinhole Exposure of Shot 155 at
A-K Gap = 0.5 cm - Quantized Mode

did not show much improvement. There still were sideways spot motion and late time shorts just as on bad REBA shots even though the energy in the beam was much higher than in the case just discussed. The current of course was lower and the magnetic trapping was less effective so that the deposition annulus was much thicker. One possible explanation for the nonuniformity was that a very few whiskers exploded early in time and closed the gap in an irregular manner. We found that a highly polished (3 micron diamond grit Metadi) surface brought about no significant improvement.

Near the end of the last chapter it was suggested that the reason the Aquadag surface did not appear to be superior to the epoxy ring surface in the REBA diode was that there was not enough current from that high-impedance machine to light up all the whiskers on the Aquadag. Possibly it would work better on Hydra. Indeed it did. When the Aquadag was sprayed uniformly right over the epoxy ring surface, a more uniform beam was reproducibly obtained. The beam at the anode that was obtained with a gap of 1.27 cm on an Aquadag surface is illustrated by the pinhole diagnostics shown in Fig. 5.7 and 5.8. It is evident that there is very little azimuthal motion of the beam electrons all through the pulse. The angular distribution of electrons is very narrow at each point, and the beam is pinching only slightly. It is also true that the annulus is much thicker because more spots appear. In fact, in the quantized mode picture of Fig. 5.8 the exposed region around the periphery is caused by electrons which have gone around the outer edge of the pinhole plate. In the quantized picture the broadness of the exposed area is misleading. There is very little exposure there. It is the separation between contours and their total number that matters, not the darkness of the contour bands. This broad weak exposure is due to pinhole edge scattering and penetration.

At this point there seemed to be no obvious way to improve the beam as it emerged from the anode with the configuration as it existed at that time. Smaller A-K gaps led to nonuniform emission; larger gaps led to serious impedance mismatch, and no other cathode surface has yet been found that is superior to Aquadag. It also seemed that the second window would not be useful because, with only a slightly

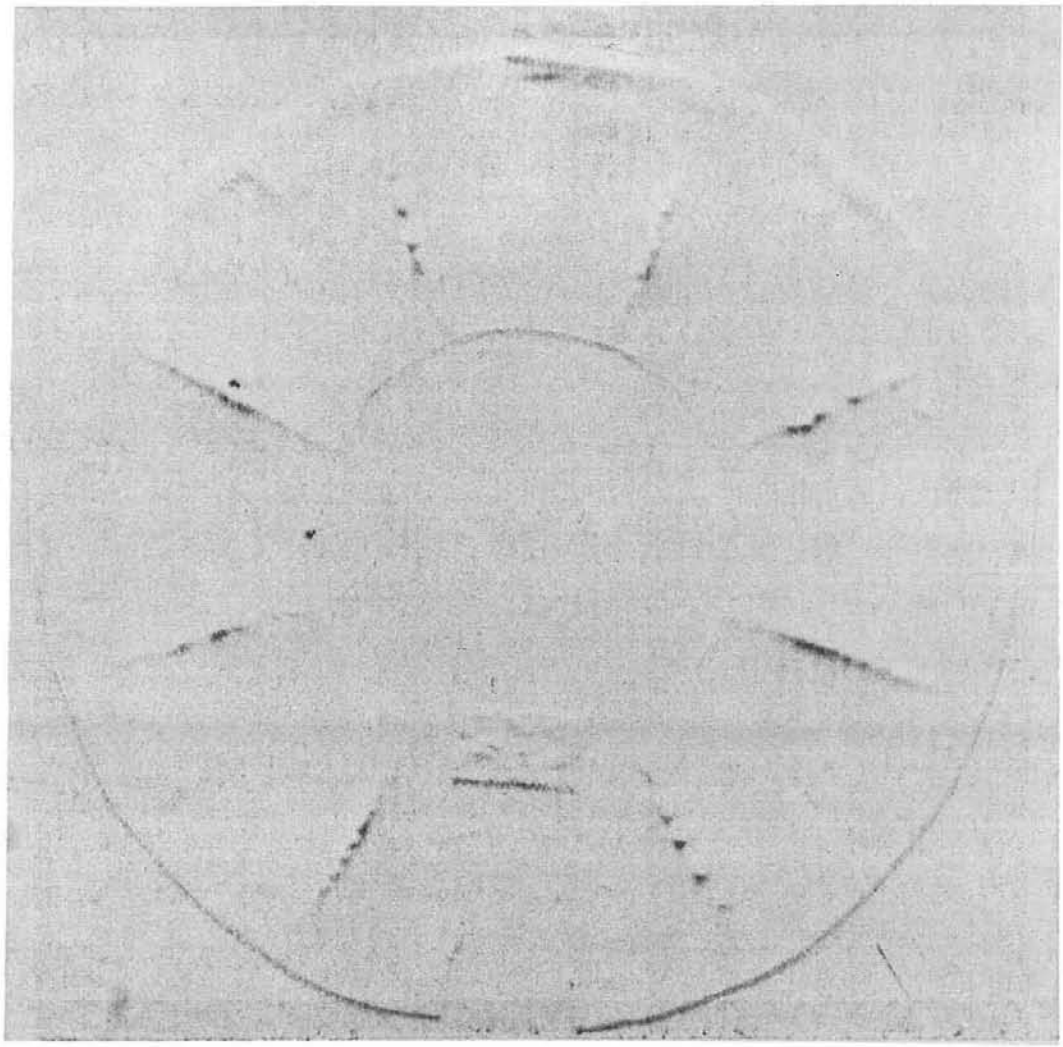

Figure 5.7 Pinhole Exposure of Shot 322 at
A-K Gap = 1.27 cm - Differential Mode

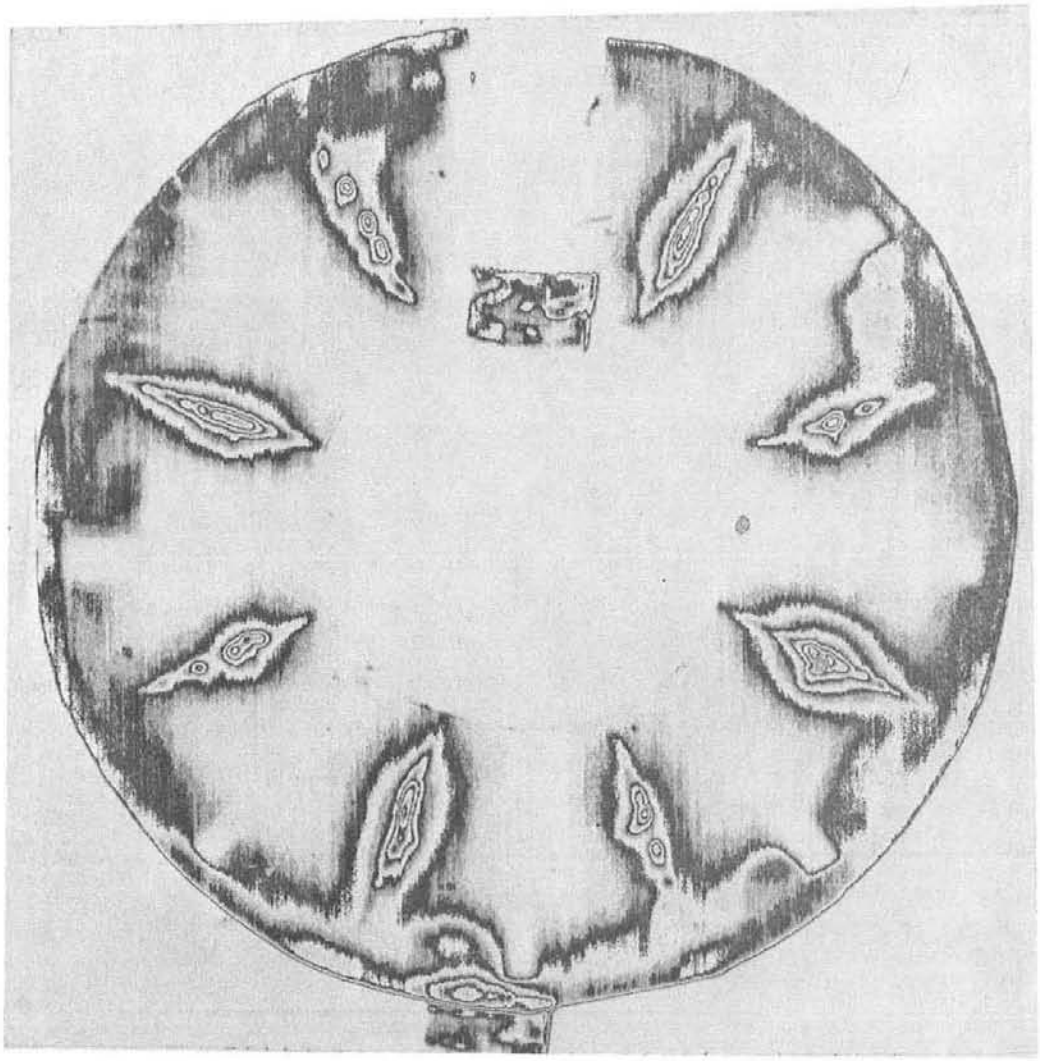

Figure 5.8 Pinhole Exposure of Shot 322 at
A-K Gap = 1.27 cm - Quantized Mode

pinched sheet, a high net current section would only increase the radial electron velocities. For these reasons a final series of shots was taken to document the transport and focusing properties of the best beam found up to that point. This was the Aquadag cathode at 1.27 cm A-K gap.

The Faraday cup calorimeter combination was being repaired at this time so that witness plates and pinhole diagnostics had to be relied upon for the measurements. They were sufficient for answering the question as to the focusability. Figure 5.9 shows the result of a pinhole measurement taken at 2 Torr at the exit of the cone. There were five 0.159 cm diameter holes in a 12 cm thick carbon plate; one in the center and four around the edge of the beam. The most striking feature about this exposure is that the beam has been separated in radius according to angular momentum. At the edge, the beam was divided into two components, one rotating to the left and one to the right. Only a minor part is going straight. The average azimuth angle of the two groups is about 16 degrees. This dosimeter was placed about 1 cm beyond the expected focal point and the beam diverged here. The transport in the channel appeared to be very efficient down to the last cone section where the beam began to damage the steel cone at a diameter of about 3.81 cm. Both the cone damage and the dosimeter showed that the beam was very uniform and azimuthally symmetric. The size of the beam and the slight vaporization of a carbon witness plate both indicate an energy density of between 200 and 300 calories/cm^2.

Conclusions about the Hydra Experiments

It would of course be of interest to document all of the features of this beam with the full array of Faraday cups, Rogowski coils, and pinhole and mapping diagnostics at each step down the cones to compare in detail with the theory developed in Part I. However, our purpose was not to verify theory but to obtain an efficiently and tightly focused drifted beam, or at least to find what limits that focusability. Both of the latter were accomplished with moderate success and with sufficient accuracy with the experiments that have been discussed here. The tests have, therefore, been discontinued.

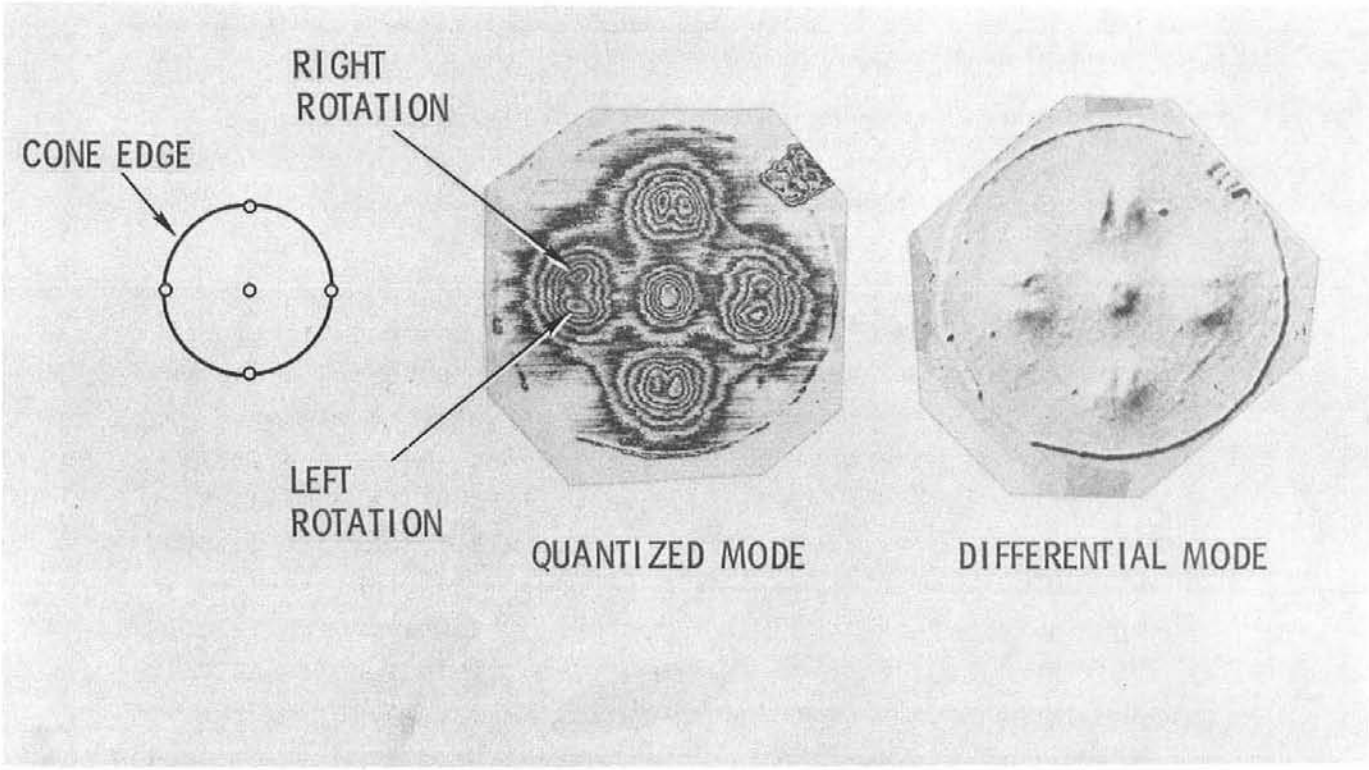

Figure 5.9 Pinhole Measurement of the Electron Angular Distribution at the Cone Exit

CHAPTER VI - DISCUSSION AND GENERAL CONCLUSIONS ABOUT THE TRIAX SYSTEM

At the present time, there are no plans to investigate the properties of this Triax system further. However, the investigation has yielded a great deal of useful information about electron beam and diode physics that has already been of considerable help in the understanding of other diode and transport physics problems encountered at this Laboratory. Some of the more important results are summarized below.

(1) If a beam of large cross section and cylindrical symmetry is to be focused with a high degree of compression, it is essential that the electrons have very low angular momentum around the axis.

(2) The theory points out an obvious, yet often ignored fact that in a cylindrically symmetric system under the influence of self-induced magnetic fields only, the outer wall has no direct effect on the beam. This is because the magnetic field is only proportional to the current inside the field point radius, $B = \mu_0 I/2\pi r$. However, if there is a conducting medium within the channel and the B field is changing, then an induced electric field is developed which can drive currents within the field point radius. This electric field is determined by the outer wall position. This fact supplies the starting point for understanding how single cones can concentrate beams.[14]

(3) Angular momentum in a concentrating beam can wash out tendencies for filamentation because of velocity shear stabilization.

(4) At gross electric field levels in the diodes of 20 kV/cm or more, plasmas are launched in the diode. If fields of about this strength are marginally reached, only a few whiskers will blow with the result that very nonuniform plasmas and very erratic beams are generated. At higher voltages the plasmas tend to be more uniform.

(5) Even though the theory is simple, it points up the importance of taking into account the time dependence of the typical pulsed beams in order to explain the principal features of beam transport in conducting boundaries. Without it, the presence of image forces cannot be justified.

(6) Probably for any beam focusing configuration, it is important to have an integrated design for the cathode, anode, transport system, and focusing system. The generated beam must be properly formed for injection into the transport and focusing system or the beam will be lost in one way or another.

(7) The proof that a prepulse will launch plasmas that cause erratic and shorted shots, and the use of methods to reduce that prepulse so that smaller gaps could be used, served for us as an early introduction to two fields that have become very important to this laboratory. First, with smaller gaps, small area cathodes could be used to generate higher density beams and experiments with small metal rods were being carried out when Morrow's article[11] about small glass rods appeared in the literature. Our experience with the metal rods led us to the conclusion that the glass rod acted as a prepulse isolator which broke down to become a good conductor when the main voltage came along. The electrons were then accelerated from the tip as from a normal metal rod. This interpretation differed from Morrow's opinion that the electrons were accelerated all along the rod. Soon after this Bradley and Kuswa[10] used the glass rods to study ion acceleration in these diodes. Second, the close gaps with larger area cathodes caused very tight diode pinches to be formed on the REBA accelerator. (This was a 7.5 cm diameter flat carbon cathode with an A-K gap of 1.27 cm.) With this diode, carbon was vaporized from a small area target for the first time at Sandia. This work was never reported and we did not realize immediately that a "super pinch" was being observed. Later, in a different configuration, Yonas, et al.,[15] recognized and

explained the new feature of this diode pinch which has now become the primary mechanism by which this Laboratory hopes to achieve nuclear fusion with electron beams.

(8) The elimination of the prepulse plasma did not solve the diode plasma problem because it was after this that apparent velocities of 10 cm/μsec were discovered. The measurements with streak cameras[10] and holography[16,17] later substantiated these findings.

There are two major factors that have limited the focusability of this Triaxial diode up to this stage of development. First, the very rapid diode plasma velocities have precluded us from operating at the small A-K gaps that are necessary for narrow sheet beams. Second, the intrinsic uniformity and spatial coherence of the emission from the cathode surface is not good enough to allow areal compression greater than 10, even with the best surfaces now available. Solutions of both these problems are still being sought but presently not with the Triaxial geometry. For example, experiments are being made on the Nereus accelerator at Sandia on the properties of diode plasmas as a function of electrode material and electrode cleanliness (amount of low-Z surface contaminant). Preliminary results indicate that a clean Ta anode plasma moves more slowly than that from a dirty Al plate.

References

1. J. G. Kelly and W. H. Vandevender, Transmission and Compression of an Intense Relativistic Electron Beam Produced by a Converging Annular Diode with Return Current Feedback Through the Cathode - Part I: Theory and Computer Computations, SAND-75-0399, Sandia Laboratories, Albuquerque, New Mexico, February 1975.

2. O. L. Johnson, REBA, A Pulsed Electron Beam Generator, SC-DR-70-872, Sandia Laboratories, Albuquerque, New Mexico, December 1970.

3. D. W. Forster, J. C. Martin, et al., Electron Beam Diagnostics using X-rays, SSWA/JCM/714/162, Atomic Weapons Development Establishment (AWRE), Aldermaston, England, April 1971.

4. R. K. Parker and R. E. Anderson, Record of the 11th Symposium on Electron, Ion and Laser Beam Technology, Ed., R. F. M. Thornley, San Francisco Press, Inc., San Francisco, California, 453 (1971).

5. L. P. Bradley, et al., Record of the 11th Symposium on Electron, Ion and Laser Beam Technology, Ed., R. F. M. Thornley, San Francisco Press, Inc., San Francisco, California., 533 (1971).

6. J. G. Kelly and L. P. Bradley, Pinhole Diagnostics for Direct Measurements of Localized Angular Distributions in Relativistic High Current Electron Beams, SC-RR-72 0058, Sandia Laboratories, Albuquerque, New Mexico, January 1972.

7. L. P. Bradley, J. G. Kelly, et al., "High υ/γ Electron Beam Injection," Bull. Amer. Phys. Soc., Ser. II, Vol. 16, No. 11, 1228 (1971).

8. L. A. Harrah, "Pulsed Electron Beam Energy Deposition Profiles Using Solid Radiation Sensitive Plastics," IEEE Trans. Nucl. Sci., Vol. NS-17, 278 (1970).

9. L. P. Bradley and C. W. Kuswa, Phys. Rev. Lett., 29, 1441 (1972).

10. D. L. Morrow, et. al., Appl. Phys. Lett., 8, No. 10, 441 (1971).

11. A. J. Toepfer and L. P. Bradley, J. Appl. Phys., 43, No. 7, 3033 (1972).

12. T. H. Martin, "Hydra Electron Beam Generator," IEEE Trans. Nucl. Sci., NS-20, No. 3, 289 (1973).

13. C. L. Olsen, Phys. Fluids, 16, No. 4, 529 (1973).

14. G. Yonas, K. R. Prestwich, J. W. Poukey and J. R. Freeman, Phys. Rev. Lett., 30, 164 (1973).

15. L. P. Mix, J. G. Kelly, G. W. Kuswa, D. W. Swain, and J. N. Olsen, J. Vac. Sci. and Tech., 10, 951 (1973).

16. J. G. Kelly, L. P. Mix, J. Appl. Phys., 46, 1084 (1974).

DISTRIBUTION:

U.S. Energy Research and Development
Administration
CTR Division
Washington, DC 20545
Attn: R. L. Hirsch (1)
B. Miller (1)
J. Decker (1)

U.S. Energy Research and
Development Administration
Laser Division
Washington, DC 20545
Attn: G. W. Kuswa (1)

Cornell University
Department of Applied Physics
Ithaca, NY 14850
Attn: H. Fleischmann (1)
B. Kusse (1)
T. Lockner (1)
C. Wharton (1)

Massachusetts Institute of Technology
Cambridge, MA 02139
Attn: G. Bekefi (1)
B. Coppi (1)
R. Taylor (1)

Physics Department
University of California
Irvine, CA 92664
Attn: N. Rostoker (1)
G. Benford (1)

General Atomics
Pure and Applied Physics Sciences
P. O. Box 608
San Diego, CA 92101
Attn: R. Freeman (1)

Holifield National Laboratory
P. O. Box Y
Oak Ridge, TN 37830
Attn: J. Clarke (1)
R. Dory (1)
L. Berry (1)

Distribution:

Lawrence Livermore Laboratory
P. O. Box 808
Livermore, CA 94550
Attn: R. Briggs (1)
D. Prono (1)

Los Alamos Scientific Laboratory
P. O. Box 1663
Los Alamos, NM 87544
Attn: L. E. Thode (1)

Maxwell Laboratories, Inc.
9244 Babboa Avenue
San Diego, CA 92123
Attn: A. Kolb (1)

Naval Research Laboratory
Code 7708
Washington, DC 20375
Attn: D. Hammer (1)
C. Kapetanakos (1)
J. Cooperstein (1)

Physics International Co.
2700 Merced Street
San Leandro, CA 94709
Attn: S. Putnam (1)
J. Benford (1)
V. Bailey (1)

5000 A. Narath
5100 J. K. Galt
5200 E. H. Beckner
5230 M. Cowan
5231 J. H. Renken
5231 W. H. Vandevender (5)
5232 L. D. Posey
5232 R. L. Schuch (2)
5233 M. J. Forrestal
5240 G. Yonas
5241 J. R. Freeman
5241 K. D. Bergeron
5241 M. J. Clauser
5241 A. V. Farnsworth, Jr.
5241 G. R. Hadley
5241 C. L. Olson
5241 J. W. Poukey
5241 M. A. Sweeney
5241 M. M. Widner

Distribution:

5241 T. P. Wright
5242 A. J. Toepfer
5242 W. B. Boyer
5242 J. Chang
5242 S. A. Goldstein
5242 C. W. Mende
5242 P. A. Miller
5242 L. P. Mix
5242 J. N. Olsen
5242 F. C. Perry
5242 D. W. Swain
5245 T. H. Martin
5245 M. Aker
5245 D. L. Johnson
5245 D. H. McDaniel
5245 K. R. Prestwich
5245 J. J. Ramirez
5245 J. P. Vandevender
5400 A. W. Snyder
5410 D. J. McCloskey
5420 J. V. Walker
5423 J. E. Powell
5423 J. G. Kelly (5)
5423 D. A. McArthur
5430 R. M. Jefferson
5440 H. D. Sivinski
5700 J. H. Scott
5800 R. S. Claassen
9330 A. J. Clark, Jr.
9331 P. H. Adams
9331 N. R. Keltner
8266 E. A. Aas (2)
3141 C. A. Pepmueller (Actg.) (5)
3151 W. L. Garner (3)
for ERDA/TIC (Unlimited Release)
ERDA/TIC (25)
(R. P. Campbell, 3171-1)